PLOS ONE

RESEARCH ARTICLE

Calcium imaging in intact mouse acinar cells in acute pancreas tissue slices

Urška Marolt[1]*, Eva Paradiž Leitgeb[2], Viljem Pohorec[2], Saška Lipovšek[2,3,4], Viktória Venglovecz[5], Eleonóra Gál[5], Attila Ébert[5], István Menyhárt[5], Stojan Potrč[1], Marko Gosak[2,3], Jurij Dolenšek[2,3]*, Andraž Stožer[2]*

1 Clinical department for abdominal and general surgery, University Medical Centre Maribor, Maribor, Slovenia, **2** Institute of Physiology, Faculty of Medicine, University of Maribor, Maribor, Slovenia, **3** Faculty of Natural Sciences and Mathematics, University of Maribor, Maribor, Slovenia, **4** Faculty of Chemistry and Chemical Engineering, University of Maribor, Maribor, Slovenia, **5** Department of Pharmacology and Pharmacotherapy, University of Szeged, Szeged, Hungary

* ursusmarolt@gmail.com (UM); jurij.dolensek@um.si (JD); andraz.stozer@um.si (AS)

Citation: Marolt U, Paradiž Leitgeb E, Pohorec V, Lipovšek S, Venglovecz V, Gál E, et al. (2022) Calcium imaging in intact mouse acinar cells in acute pancreas tissue slices. PLoS ONE 17(6): e0268644. https://doi.org/10.1371/journal.pone.0268644

Editor: Ilse Rooman, Vrije Universiteit Brussel, BELGIUM

Received: December 17, 2021

Accepted: May 4, 2022

Published: June 3, 2022

Data Availability Statement: All relevant data are within the paper and its Supporting Information files.

Funding: Medical Centre Maribor (project IRP-2015/02-04). The authors also acknowledge support from the Slovenian Research Agency (research core funding nos. P3-0396 and I0-0029, as well as research projects nos.J3-3077, N3-0133, N3-0170, J3-9289, J3-2525, N3-0048) and National Office for Research, Development and Innovation (SNN134497 to VV). The funders had

Abstract

The physiology and pathophysiology of the exocrine pancreas are in close connection to changes in intra-cellular Ca^{2+} concentration. Most of our knowledge is based on *in vitro* experiments on acinar cells or acini enzymatically isolated from their surroundings, which can alter their structure, physiology, and limit our understanding. Due to these limitations, the acute pancreas tissue slice technique was introduced almost two decades ago as a complementary approach to assess the morphology and physiology of both the endocrine and exocrine pancreas in a more conserved *in situ* setting. In this study, we extend previous work to functional multicellular calcium imaging on acinar cells in tissue slices. The viability and morphological characteristics of acinar cells within the tissue slice were assessed using the LIVE/DEAD assay, transmission electron microscopy, and immunofluorescence imaging. The main aim of our study was to characterize the responses of acinar cells to stimulation with acetylcholine and compare them with responses to cerulein in pancreatic tissue slices, with special emphasis on inter-cellular and inter-acinar heterogeneity and coupling. To this end, calcium imaging was performed employing confocal microscopy during stimulation with a wide range of acetylcholine concentrations and selected concentrations of cerulein. We show that various calcium oscillation parameters depend monotonically on the stimulus concentration and that the activity is rather well synchronized within acini, but not between acini. The acute pancreas tissue slice represents a viable and reliable experimental approach for the evaluation of both intra- and inter-cellular signaling characteristics of acinar cell calcium dynamics. It can be utilized to assess many cells simultaneously with a high spatiotemporal resolution, thus providing an efficient and high-yield platform for future studies of normal acinar cell biology, pathophysiology, and screening pharmacological substances.

no role in study design, data collection, analysis, and preparation of the manuscript.

Competing interests: The authors have declared that no competing interests exist.

Introduction

With increasing numbers of patients suffering from diabetes mellitus, pancreatitis, and pancreatic cancer, understanding normal and pathological pancreas physiology is becoming more and more important [1–4]. The treatment options for these diseases are limited and they are all characterized by shorter life expectancy, poorer quality of life, and higher morbidity after treatment attempts [5, 6]. The pancreas is a bifunctional gland consisting of exocrine acini and ducts and endocrine islets of Langerhans [7]. The former regulates the digestive breakdown of energy-rich polymers in food, and the latter coordinates the postprandial storage and use of energy-rich nutrients, as well as their controlled interprandial release from internal stores [8–11]. The exocrine pancreas represents more than 90% of total organ volume and comprises acinar and ductal cells that secrete enzymes, their precursors (zymogens), and a bicarbonate-rich fluid. The remaining $< 10\%$ of the organ are endocrine cells (1–4%) and interstitial or mesenchymal components: the blood and lymphatic vessels, nerves, fibrous tissue, and immune cells [12–19]. The pancreatic exocrine function is stimulated by neurotransmitters and hormonal secretagogues, for instance, acetylcholine (ACh) and cholecystokinin (CCK). These two molecules exert their effects through different intra-cellular mediators, which liberate Ca^{2+} from intra-cellular stores, the endoplasmic reticulum (ER), and acid Ca^{2+} pools into the cytosol [20, 21]. Under physiological conditions, the rise of intra-cellular Ca^{2+} concentration ($[Ca^{2+}]_i$) is mainly confined to the apical region in the form of short-lasting and repetitive local $[Ca^{2+}]_i$ signals responsible for exocytosis and acinar fluid secretion. Eventually, the secretagogue stimulus is sufficient to raise $[Ca^{2+}]_i$ concentration globally towards the basal cell pole, which influences ion transport, protein synthesis, and cell metabolism [22–25]. $[Ca^{2+}]_i$ oscillations propagate between cells via gap junctions (Cx24, Cx32) and are believed to be synchronized among cells in the same acinus [25–30]. Sustained elevation in $[Ca^{2+}]_i$ concentration evoked by pathological agents, such as bile acids, fatty acids, and non-oxidative alcohol metabolites (fatty acid ethyl esters), leads to a bioenergetic collapse of the acinar cell, resulting in inappropriate intra-cellular trypsin activation, activation of nuclear factor-κB, cytoskeletal damage, mitochondrial dysfunction, vacuolization, and necrosis, causing cell injury and acute pancreatitis [31–35].

The key research endeavors to understand the intra-cellular mechanisms responsible for acinar cell enzyme synthesis and secretion were performed on cell lines, freshly isolated acinar cells, and isolated pancreatic acini [36, 37]. Isolation protocols employed in these methods involve digestion by enzymes, a procedure that leads to structural and functional changes, manifested as loss of microvilli and surface receptors, changes in membrane potential, upregulation of cytokines and chemokines, protein kinase activation, and reduced ACh-stimulated secretion of zymogene granules [38–40]. Furthermore, cell-to-cell contacts, which are crucial for normal pancreatic exocrine function, become interrupted during isolation of single cells [30, 41–45]. Moreover, isolation of acini does not enable paracrine-endocrine interactions, has been demonstrated to prevent contacts with the extracellular matrix and is associated with acinar cell transdifferentiation, which, taken together, ultimately alters their physiology [38, 44, 46–53]. To overcome at least some of the above stated drawbacks and enable the investigation of exo- and endocrine cells in a more natural environment, in analogy with successful similar approaches in other tissues [54–57], the acute pancreas tissue slice technique was introduced in 2003 [19, 39, 50, 58, 59]. The main advantage of this approach is the short preparation time without the need for overnight culturing, with the first slices being available for experiments in less than an hour [50, 60, 61]. The preparation involves minimum mechanical stress, no exogenous enzymatic degradation, the morphological and physiological features are preserved, and with some adaptations, the slices can be used for long periods of time [59]. The tissue slices

were initially employed for *in situ* studies of endocrine beta and alpha cells [58, 62–64], and later also for acinar and ductal cells [50, 65–67] and other types of cells in the pancreas [58, 59, 65, 68–72].

With regard to $[Ca^{2+}]_i$ signaling in acinar cells, there is an open question as to whether the $[Ca^{2+}]_i$ elevations elicited by ACh and other secretagogues in isolated cells and clusters occur in undissociated preparations, and if they do, what are their properties [35]. To the best of our knowledge, it has not been possible to monitor $[Ca^{2+}]_i$ changes in acini *in vivo* so far [35]. One study demonstrated $[Ca^{2+}]_i$ oscillations in intact isolated lobuli [73] and three previous studies in acute pancreas tissue slices mention acinar cell $[Ca^{2+}]_i$ dynamics, two in mouse [59, 74] and one in human tissue [66]. However, these studies did not aim to quantify the responses to different levels of stimulation systematically or to assess the degree of intra- and inter-acinar heterogeneity and coupling on a large number of cells. Additionally, the spatiotemporal resolution was typically too low to enable single-cell resolution and reliable determination of oscillation properties [66]. In the present study, we therefore specifically aimed at filling this gap in our knowledge and set out to analyze the responses of acinar cells to stimulation with a wide range of concentrations of the physiological agonist ACh, with particular emphasis on the coding properties of these responses, their heterogeneity, and coupling within and between acini. Additionally, we analyzed the response to cerulein, an analogue of CCK, to demonstrate that the acinar cells in the acute pancreatic tissue slice respond to both secretagogues, and to compare their influence on active time of acinar cells. We demonstrate that confocal microscopy in conjunction with the acute pancreas tissue slice represents a viable and reliable experimental approach to evaluate both intra- and inter-cellular $[Ca^{2+}]_i$ signaling parameters of multiple acinar cells simultaneously, with high spatiotemporal resolution. It therefore provides a very practical platform for future high-throughput studies of normal acinar cell biology, pathophysiology, and for screening pharmacological substances.

Materials and methods

Animals

The tissue slices were acquired from C57BL/6J mice with the permission of the Veterinary Administration of the Republic of Slovenia (U34401-12/2015/3), following their recommendations, restrictions, and acts. The study was approved by the National Medical Ethics Committee of Slovenia (0120-369/2015-2). Mice of both sexes (6 females and one male) were kept in identical caging conditions (12:12 day to night ratio, standardized cage ventilation, standardized cages, and food) and sacrificed at 4 to 6 months with non-fasting glucose levels at 6.8 mmol/l-10.1 mmol/l.

Chemicals and solutions

For tissue slice preparation, 1.9% low-melting-point agarose (Lonza Rockland Inc., Rockland, Maine, USA) dissolved in extracellular solution (ECS) was used. The ECS consisted of 125 mM NaCl, 26 mM $NaHCO_3$, 6 mM glucose, 6 mM lactic acid, 3 mM myo-inositol, 2.5 mM KCl, 2 mM Na-pyruvate, 2 mM $CaCl_2$, 1.25mM NaH_2PO_4, 1mM $MgCl_2$ and 0.5 mM ascorbic acid, and was constantly bubbled with carbogen (v/v 95% O_2, 5% CO_2) to adjust pH to 7.4. The HEPES-buffered saline was composed of 150 mM NaCl, 10mM HEPES, 6 mM glucose, 5 mM KCl, 2 mM $CaCl_2$, 1mM $MgSO_4$, titrated to pH = 7.4 with 1 M NaOH. The dye-loading solution for confocal fluorescent imaging was composed of: 6 μM Oregon Green 488 BAPTA-1 AM Ca^{2+} dye (OGB-1 Invitrogen, Eugene, Oregon, USA) or Calbryte 520 AM Ca^{2+} dye (AAT Bioquest, Sunnyvale, California, USA), 0.03% Pluronic F-127 (w/v), and 0.12% dimethylsulfoxide (v/v), dissolved in HEPES. Stimulus solution was prepared by adding Acetylcholine chloride (ACh, ≥

99% purity, TLC) at indicated concentrations to the ECS. All chemicals were purchased from Sigma-Aldrich (St. Louis, Missouri, USA), unless specified otherwise.

Tissue slice preparation

Tissue slices were prepared as described in detail previously [58, 61, 70, 75]. A flowchart summarizing the main steps of the protocol is depicted in Fig 1. Briefly, following exposure to CO_2 and cervical dislocation, laparotomy was performed and the major duodenal papilla was identified and clamped. Low-melting-point 1.9% agarose at 40˚C was injected into the proximal common bile duct in order to fill the pancreas retrograde. Immediately after injection the pancreas was extracted and cooled with ice-cold ECS. We dissected the tissue to ~ 2 mm^3 tissue blocks, removed connective and vascular tissue, and embedded it into the agarose. Blocks of agarose-injected and embedded tissue were cut at 0.08 mms^{-1} and 90 Hz to 140 μm thick slices in the ice-cold ECS solution (VT 1000 s Vibratome, Leica, Nussloch, Germany). The tissue slices were immersed into the dye-loading solutions (OGB-1 or Calbryte 520 AM) for 60 minutes on an orbital shaker (50 turns min-1) at room temperature (RT). We kept the tissue slices in HEPES solution at RT until further use for calcium imaging, electron microscopy, LIVE/DEAD assays, and immunofluorescent staining.

LIVE/DEAD assay

To assess cell viability, the LIVE/DEAD® Viability/Cytotoxicity Kit (Invitrogen, Thermo Fisher Scientific, Waltham, USA) double staining kit was used. In brief, we labeled the cells

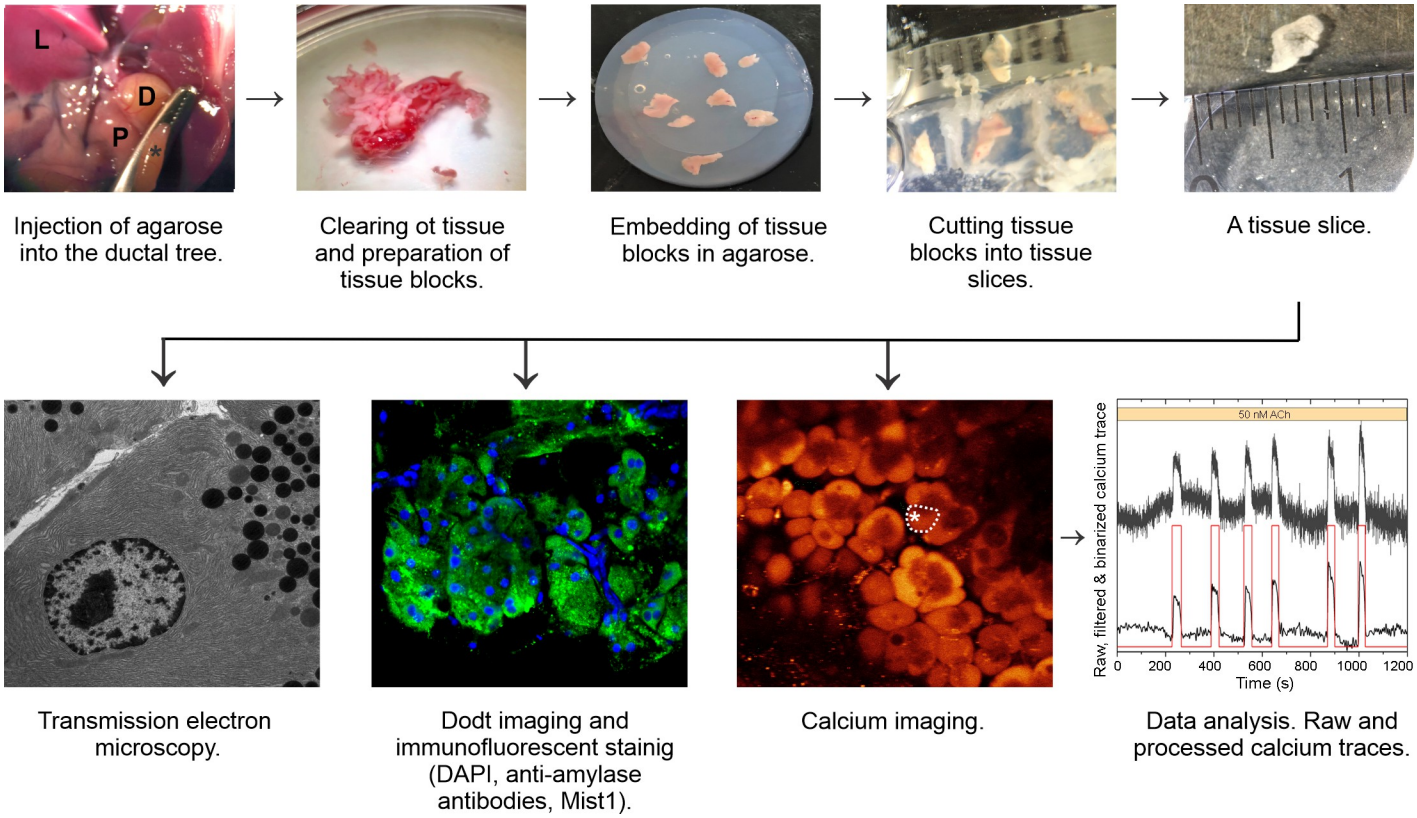

Fig 1. Flowchart for studying calcium responses in acinar cells in mouse pancreas tissue slices, from the injection of agarose into the ductal tree of the mouse pancreas and preparation of tissue slices to structural and functional imaging with data analysis. L, liver; P, pancreas; D, duodenum; asterisks, clamped major duodenal papilla.

https://doi.org/10.1371/journal.pone.0268644.g001

with calcein-AM and ethidium homodimer-1 (EthD-1), whereby calcein-AM stains viable cells with green fluorescence and EthD-1 stains dead cells with red fluorescence. The fluorescent dyes were excited at 488 nm using Leica TSC SP5 AOBS Tandem II upright confocal system (20x water immersion, NA 1.0) or a Leica TCS SP5 DMI6000 CS inverted confocal system (20X HC PL APO Oil, NA 0.7). Emission spectra were collected at 520 ± 20 nm for calcein-AM and 680 ± 60 nm for EthD-1 [76]. Z-stacks were obtained using the LAS AF software (Leica systems) and analyzed using Fiji.

Transmission Electron Microscopy (TEM)

For TEM, acutely prepared tissue slices were fixed in 2.45% (v/v) glutaraldehyde and 2.45% (v/v) paraformaldehyde in 0.1 M sodium cacodylate buffer (pH = 7.4) at RT for 4 hours and at 4˚C for 16 hours. After fixation, the pieces were washed out with 0.1 M sodium cacodylate buffer (pH = 7.4) at RT for 3 hours and post-fixed with 2% OsO_4 at RT for 2 hours. Tissue dehydration followed with step-up ethanol concentration exposure for 30 minutes (concentrations of ethanol used; 50%, 70%, 90%, 96%, and 100%) and embedded in the TAAB epoxy resin (Agar Scientific). Ultra-thin sections of 75 nm were transferred onto copper grids, stained with uranyl acetate and lead citrate, and examined using a Zeiss EM 902 transmission electron microscope.

Amylase secretion assay

Amylase secretion measurements were carried out based on the protocol described by Marciniak et al. 2013 [59]. Briefly, each slice was incubated in 500 μl incubation buffer with or without 0.1 nM cerulein (for stimulated secretion) for 30 min at 37˚C. The supernatant was removed for subsequent measurements of amylase content. The slices were then incubated in 500 μl incubation buffer containing 3% Triton-X-100 for 10 min at room temperature with 1 min thorough vortexing. The debris were centrifuged, and the supernatant was removed. Amylase content of the supernatants was measured using a commercial colorimetric kit (Diagnosticum, Budapest, Hungary) and a Biosan HiPo MPP-96 microplate photometer (Biocenter, Szeged, Hungary) [59].

Immunofluorescent staining and imaging

The immunofluorescent staining was performed in 6-well culture plates in a batch of tissue slices separated from the ones for calcium imaging. The wells were lined with parafilm that prevented adhesion of slices to the bottom of the plate and allowed incubation in a relatively small volume. Pancreatic tissue slices were fixed in 4% (v/v) paraformaldehyde for 2 h at 4˚C while shaking, followed by washing five times for 10 min with PBS containing 0.3% (v/v) Triton X-100, at RT. Slices were incubated with a blocking buffer (10% (v/v), goat serum, and 0.3% (v/v) Triton X-100 dissolved in PBS for 2 h at RT followed by immunofluorescence staining with mouse monoclonal anti-amylase antibody (1:100 dilutions, Santa Cruz, Cat. No.: sc-514229) or rabbit monoclonal Mist-1/ bHLH15 antibody (1:100 dilution, Cell Signaling Cat. No. 14896T) overnight at 4˚C. Slices were afterward washed five times with PBS and incubated with the secondary antibody, Alexa Fluor 488 goat anti-mouse (1:400 dilutions, Thermo Fisher Scientific, Cat. No.: A28175), Alexa Fluor 647 goat anti-rabbit (1:500 dilutions, Thermo Fisher Scientific, Cat. No. A28175) and 4', 6-diamidino-2-phenylindole (DAPI; 2.5 μg/ml)) for 2h at RT while shaking. Slices were then washed six times for at least 10 min with PBS and kept in PBS at 4˚C in the dark until imaging. For imaging, tissue slices were fixed to the bottom of a 35 mm glass dish with an anchor. Immunofluorescent images were acquired with a Zeiss LSM 880 confocal laser scanning microscope (Carl Zeiss Technika Kft., Budaörs, Hungary) using 40

x objective lens (Plan-Apochromat 40x/1.4 oil) with a z step of 1 μm (10 confocal images @ 2048 x 2048 pixels).

Calcium imaging

Immediately before imaging, we transferred individual tissue slices into a temperature-controlled (37˚C) recording chamber of the confocal microscope. A peristaltic pump-based system perfused the recording chamber with ECS, and stimulation was performed by manually switching the system inlet between solutions. Two step-wise concentration-ramp protocols with ACh (prestimulatory 1 minute followed by 5 minutes per step) were applied: either the 5 nM, 10 nM, 25 nM, and 50 nM, spanning sub-physiological to physiological values (low protocol), or the 50 nM, 100 nM, 250 nM, 500 nM, and 1000 nM, spanning physiological to supra-physiological values (high protocol). In either case, a washout period was allowed to detect the deactivation of acinar cells. As a pilot study, we tested higher ACh concentrations of 10 μM in 2 slices and 100 μM in 4 slices. Additionally, a single cerulein protocol was used with 10 pM, 100 pM, and 1000 pM concentrations, which lies within the range of previously used concentrations [59]. A single stimulation protocol was performed per slice (ACh: 12 slices for the low protocol, 13 slices for the high protocol, both from 5 animals; cerulein: 11 slices, 2 animals).

The $[Ca^{2+}]_i$ dynamics were imaged with a Leica TSC SP5 AOBS Tandem II upright confocal system (20x water immersion, NA 1.0) or a Leica TCS SP5 DMI6000 CS inverted confocal system (20X HC PL APO Oil, NA 0.7) at a resolution of 5 Hz and 256 x 256 pixels or 10 Hz and 512 x 512 pixels for the higher-resolution recordings employed to detect possible apical-to-basal spreading of signal within cells. The employed Ca^{2+} dyes OGB-1 and Calbryte 520 AM were excited with the Argon 488 laser line, and emitted fluorescence was collected in the range of 500–700 nm (Leica HyD detector). Calbryte 520 AM was used to be better able to detect possible apical-to-basal differences in signals (S1 Fig) due to its resistance against extrusion from the cell, better signal to noise ratio, lower resting fluorescence with a high increase in fluorescence upon binding $[Ca^{2+}]_i$, and a larger mean number of events detected per cell per second compared to OGB-1 [77, 78]. Both Ca^{2+} dyes reported similar $[Ca^{2+}]_i$ oscillations and the type of the dye employed did not influence the results (see S2 Fig).

Processing of calcium signals and data analyses

Regions of interest (ROIs) were selected manually off-line, based on morphological characteristics, described as a single layer of pyramidal cells concentrically distributed around the intercalate duct, and characteristic $[Ca^{2+}]_i$ dynamics, using the Leica LAS AF software, and exported as time series data. To identify an acinus or acinar cells in the tissue slice, scanning gradient (Dodt) contrast [79], using the 488 nm excitation laser and transmitted light detector, was used to recognize cell boundaries and apical poles (S1B Fig). Additionally, basal differences in signal intensities between cells, as well as qualitative differences in stimulated signals between acini and temporal delays between signals in individual cells from the same acinus helped distinguish individual acini and cells (S1C Fig). Further analysis of the time series data was performed using custom code in MATLAB/Python scripts (MathWorks, Inc., Massachutesetts, Germany and Python Software Foundation, Beaverton, USA). A combination of linear and exponential fitting of the data accounted for photobleaching, and the data are presented as $F(t)/F_0(t)$, where F denotes the raw signal at time point t and F_0 the fitted baseline value at the same time point. Subsequently, the data were filtered with a zero-lag digital filter to reduce noise levels and other artefacts. Binarization of data was performed based on the onsets, peaks, and endings of oscillations. Cells that failed to exhibit sufficient signal/noise ratios to allow binarization were discarded from further analysis. The binarized data was used to calculate the

parameters of the acinar response: the average frequency, the average duration, the average relative active time and the average coefficient of the inter-oscillation interval variability (*IOIV)*. Specifically, the average relative active time was determined as the fraction of 1 (i.e., "on" states) in the binarized signals, reflecting thereby the average fraction of time that cells spend in an active state with increased $[Ca^{2+}]_i$. The coefficient of inter-oscillation interval variability was defined as the ratio between the standard deviation of inter-oscillation interval lengths and the corresponding mean interval length [80]: $IOIV_i = SD(TO_i)/<TO_i>$ where TO_i stands for the sequence of intervals between individual oscillations in the *i*-th cell. Altogether, we pooled 625 acinar cells from 214 acini in experiments with ACh and 606 acinar cells from 180 acini in experiments with cerulein. For the quantification of acinar cell synchronicity, we calculated the coactivity coefficient. This metric marks the overlap of binarized activity between different cell pairs [81]. The values of the coactivity encode the degree of cellular synchronization, whereby 0 indicates completely independent and non-overlapping activity and 1 a complete overlap between the binarized signals of a given cell pair. Coactivity coefficients between all cell pairs served also as a basis for the construction of the functional connectivity network, which features synchronous inter-cellular activity patterns [69, 81, 82].

Statistical analyses

Statistical analyses were performed with SigmaPlot 11.0 version (Systat Software, Inc., Illinois, USA). Statistics were calculated using ANOVA on Ranks and posthoc Dunn's method. For box-plot presentations of the data, boxes determinate the interval between the 25th and the 75th percentile, whiskers denote the minimal and the maximal values, lines within the boxes indicate the median, and small squares indicate the average value. Significant differences are indicated by asterisks (*, $p<0.05$; **, $p<0.01$; ***, $p<0.001$).

Results

Acinar cell viability and morphology in pancreas tissue slices

To verify the viability and morphological integrity of acinar cells within acute mouse pancreas tissue slices following isolation, cutting, and loading of the dye, we performed a set of four different and complementary assessments of their structure and ultrastructure. First, high-resolution imaging of the OGB-1 or Calbryte 520 AM loaded tissue revealed pyramidal shaped acinar cells concentrically distributed around an intercalate duct or lumen, forming a typical acinus (Fig 2A and 2B). The dye localized more strongly to the basal pole of the cells, whereas the signal was less in the apical pole, consistent with the polarity of the acinar cells [13, 83]. Second, the slicing procedure hardly affected the viability of the acinar cells as the majority of the cells appeared viable and only a few cells close to the cutting surface appeared dead on the Live/Dead assay (Figs 2C and S3). Third, the ultrastructure of the acinar cells was retained during the slicing procedure. TEM revealed (i) oval-shaped mitochondria in the perinuclear, perigranular and subplasmalemmal region; they were characterized by a double membrane, the inner mitochondrial layer formed typical cristae, (ii) rough endoplasmic reticulum that was visualized as electron-dense parallel lines within the cytoplasm, (iii) zymogene granules visualized as electron-dense round structures, and (iv) nuclei with double electron-dense membrane and a nucleolus, all consistent with the typical acinar cell ultrastructure (Fig 2I–2K) [84–87]. Next, immunohistochemical staining revealed that the acinar cells abundantly expressed the enzyme amylase, the acinar cell end-product (Fig 2E, 2G and 2H) and stimulation of slices by 0.1 nM cerulein resulted in a significant increase in amylase secretion (Fig 2L), further corroborating the functional viability of acinar cells in the tissue slice [88, 89]. Finally, Fig 2F featuring immunofluorescence against the basic helix-loop-helix transcription factor Mist-1 shows

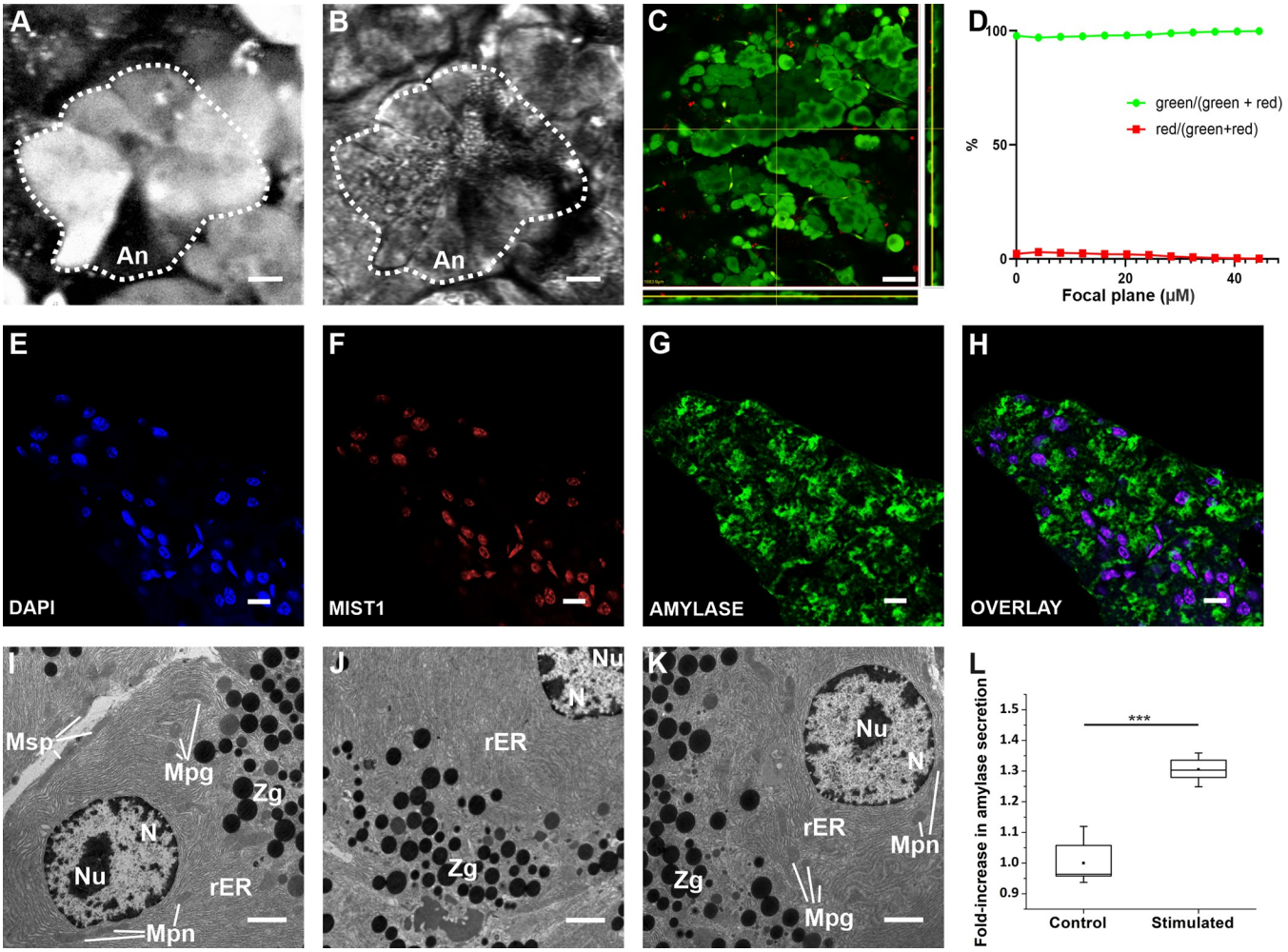

Fig 2. Morphology of acinar cells in mouse pancreas tissue slices. (A, B) High resolution confocal fluorescence images of the exocrine part of the pancreas, labeled with OGB-1 (A) and imaged with Dodt contrast (B). An; acinus is encircled by the broken line. Scale bar 10 μm. (C) A layer from a z-stack, cells were loaded with the Live/Dead dye. Side panels represent orthogonal projections of the z-stack, positioned as indicated by yellow lines. Pseudo color-coded, such that green indicates live cells and red indicates dead cells. Scale bar 50 μm. (D) The percentage of live cells in green and dead cells in red, as a function of depth of the focal plane within the slice. (E, F, G, H) Staining of nuclei with DAPI (E) and anti-Mist1 antibodies (F), and of cytoplasm with anti-amylase antibodies (G), with the overlay (H). Scale bar 10 μm. (I-K) TEM images of acinar cells from a tissue slice. Mpn, perinuclear mitochondria; Mpg, perigranular mitochondria; Msp, subplasmalemmal mitochondria; Zg, zymogen granules; N, nucleus; Nu, nucleolus; rER, rough endoplasmic reticulum. Scale bar 10 μm. (L) Quantification of amylase secretion upon stimulation by 0.1 nM cerulein, n = 6. Significant difference is indicted by asterisks (***, $p<0.001$).

https://doi.org/10.1371/journal.pone.0268644.g002

that the exocrine pancreas organization and acinar cell identity were maintained in the tissue slice *in situ*, at least over the time period during which our experiments were performed.

Dose-dependent $[Ca^{2+}]_i$ responses to ACh

We resorted to functional multicellular confocal imaging of $[Ca^{2+}]_i$ dynamics of mouse acinar cells to characterize their response to Ach and cerulein in tissue slices. A pilot study indicated that in slices, concentrations > 1000 nM saturated the acinar cell response to ACh. We detected a tonic increase in $[Ca^{2+}]_i$ in 86% of cells (n = 43) at 10 μM and in 98% cells (n = 133) at 100 μM (Fig 3). Due to the lack of oscillatory activity at concentrations > 1000 nM, we selected two step-wise protocols composed of sequentially increasing ACh concentrations: one spanning a lower (5–50 nM) and the other a higher (50–1000 nM) concentration range. A

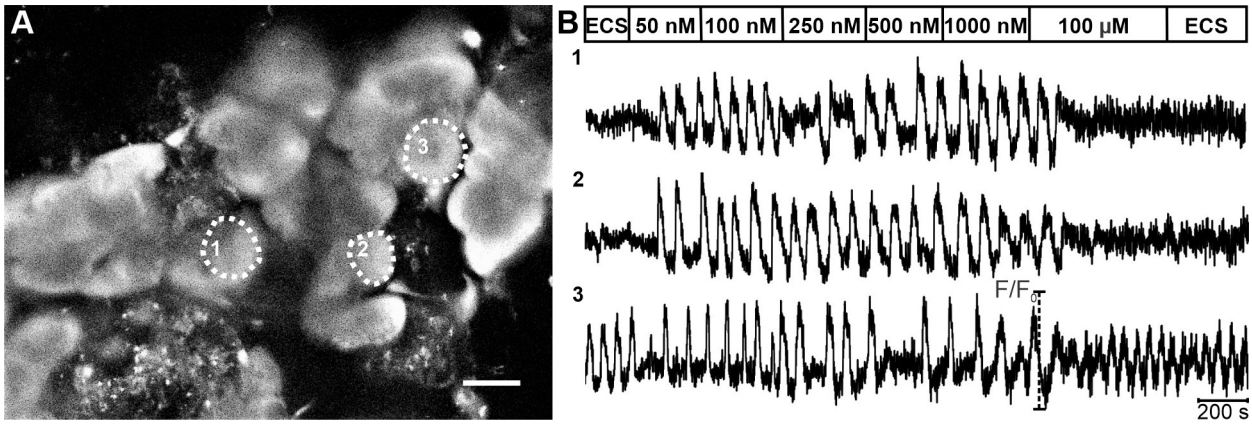

Fig 3. $[Ca^{2+}]_i$ oscillations in acinar cells upon stimulation with a ramp of ACh concentrations. (A) OGB-1 loaded acinar cells in a tissue slice. Scale bar 20 μm. (B) $[Ca^{2+}]_i$ oscillations shown here belong to the acinus marked with thin broken line and the corresponding number in (A). At the beginning and end of the protocol, extracellular solution (ECS) was used (see Materials and Methods). On average, after stimulation with 100 μm ACh, a biphasic $[Ca^{2+}]_i$ response with a rise in basal $[Ca^{2+}]_i$ level was seen in 98.5% of acinar cells. Note that in cell 3, spontaneous $[Ca^{2+}]_i$ activity was observed prior to stimulation, whereas cells 1&2 lacked spontaneous activity.

https://doi.org/10.1371/journal.pone.0268644.g003

latent period of 90–120 s was observed before cells reacted to secretagogue stimulation. In approximately half of the tested cells (54.2%, n = 339/625), no activity was detected in the non-stimulatory conditions, and the ACh stimulation provoked a response pattern consisting of oscillatory changes in $[Ca^{2+}]_i$. The remaining half of the tested cells expressed oscillatory activity prior to stimulation, while the ACh stimulation increased the frequency and/or duration of oscillations. Fig 3 shows spontaneous $[Ca^{2+}]_i$ oscillations in cell 3 and no spontaneous activity in cells 1 and 2. The response pattern was qualitatively and quantitatively similar between spontaneously active and inactive cells, and consistent with previously published data [21, 25, 90, 91].

Fig 4 compares $[Ca^{2+}]_i$ oscillations within and between acini. The pattern of activity was comparable between cells belonging to the same acinus (compare cells 1–3 in Fig 4). Comparison of $[Ca^{2+}]_i$ patterns between acini revealed great variability in terms of both frequency and duration of oscillations (compare responses of cells 4 and 5 belonging to two separate acini, with the responses of cells 1–3 from a third acinus in Fig 4). Moreover, we detected local differences in the $[Ca^{2+}]_i$ increase within an acinar cell, with the signal at the apical pole preceding the signal at the basal pole by several seconds (S1 Fig), consistent with what has been reported previously [25].

Furthermore, acinar cells responded to ACh stimulation dose-dependently, as exemplified in Fig 5. Increasing the concentration of ACh from 5 nM to 1000 nM gradually increased the frequency and the duration of individual oscillations. To quantify this dose-dependence, we measured the average frequency, duration, relative active time, and inter-oscillation interval variability of $[Ca^{2+}]_i$ oscillations (Fig 6). A significant increase in frequency and duration was observed only for some of the tested concentrations, most probably due to relatively large inter-acinar variability (Fig 6A and 6B). In an attempt to overcome the large degree of variability, we pooled the data for low (5–25 nM), intermediate (50–100 nM), and high (250–1000 nM) ACh concentration (Fig 6E and 6F). The relative increase in average oscillation frequency was larger between the low and the intermediate range (139%, median 0.007 Hz vs 0.01 Hz; $p<0.001$) than between the intermediate and the high range (127%; median 0.01 Hz vs. 0.013 Hz). Similarly, the average duration increased the most between the low and the intermediate range (139%; median 23.3 s vs. 32.1 s; $p<0.001$) and less between the intermediate and the high range (103%; median 32.1 s vs. 33 s; $p<0.01$). The overall activity of cells was robustly assessed by calculating the active time, presenting the fraction of time occupied by oscillations

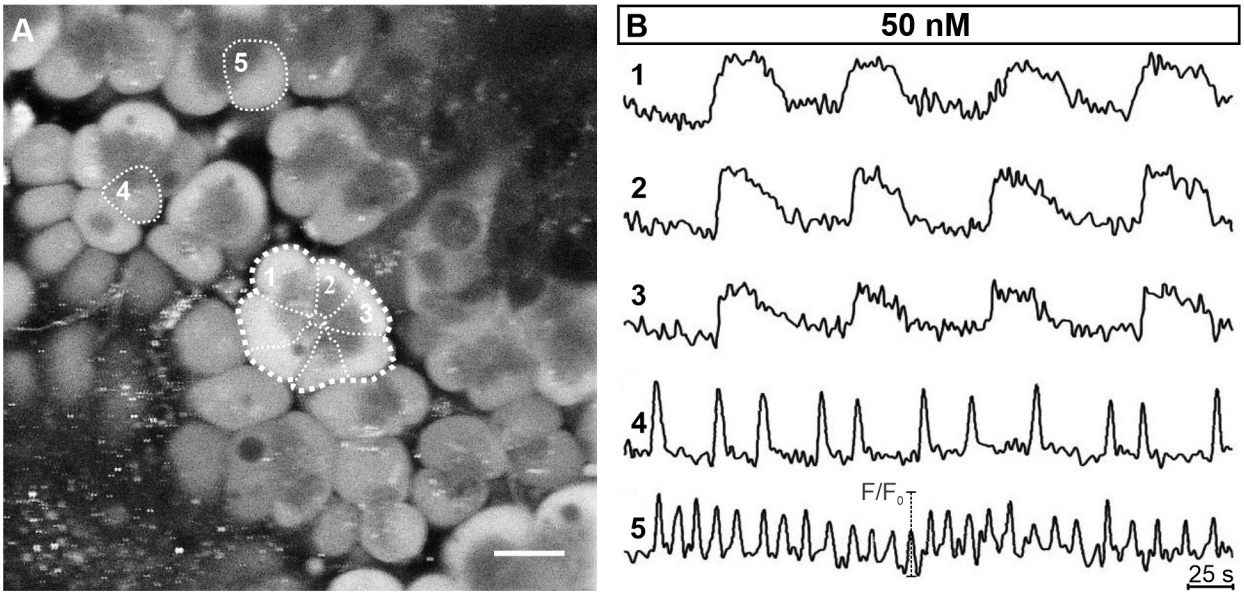

Fig 4. $[Ca^{2+}]_i$ oscillations within different acini. (A) OGB-1 loaded acinar cells in a tissue slice. Cells indicated with 1–3 belong to the same acinus (the thicker broken line marks the acinus, the thinner broken lines mark boundaries between individual acinar cells). Scale bar 20 μm. (B) The $[Ca^{2+}]_i$ activity patterns in three different acinar cells from the same acinus (1–3) and in two cells from two other distinct acini (cells 4 and 5) stimulated with 50 nM ACh. Please note that $[Ca^{2+}]_i$ oscillations were similar in shape and synchronized between cells in the same acinus but not between cells from different acini (1–3 vs. 4 vs. 5).

https://doi.org/10.1371/journal.pone.0268644.g004

or the duty time of cells, similarly to the approach in endocrine beta cells [92]. Considering the above modulation of frequency and duration and given that, the active time is a combination of both, the average relative active time correspondingly increased with increasing ACh concentrations (Fig 6C). The highest increase in the relative active time was again observed between the low and the intermediate range of ACh concentrations (163%, median 0.195 vs. 0.318; $p<0.001$, Fig 6G). Finally, to evaluate the regularity of oscillations, we calculated the coefficient of inter-oscillation interval variability. A significant decrease in interval variability was observed for the most extreme of the tested concentrations (Fig 6D), and this parameter decreased more between the low and the intermediate (139%; median 0.25 vs. 0.18; $p<0.001$, Fig 6H) compared to the decrease between the intermediate and the high range of stimulation (120%; median 0.18 vs. 0.15; $p = 0.033$).

Inter-cellular synchronization of acinar cells

As noted above, acinar cells from an acinus expressed a qualitatively more similar oscillatory pattern compared to activity in other acini (Fig 4). To quantify the level of inter-cellular synchronization, we calculated the average coactivity between pairs of cells (see Methods for detailed description and Fig 7C). First, in Fig 7A and 7B, we present a functional network of acinar cells and a raster plot of binarized activity after the tissue slice was stimulated with 50 nM ACh. Different colors of cells denote different acini. The activity was well synchronized only between cells from the same acinus, while the activity pattern differed considerably in the neighboring acini. Therefore, functional connections, reflecting well synchronized cellular activity, were established only between cell pairs within the same acini and not between the cells from the neighboring acini. Furthermore, the oscillations from the same acinus were similar also in shape (Fig 7C). Second, we computed the average coactivity coefficient to quantify the extent of synchronization within different acini and for different stimulation levels. The

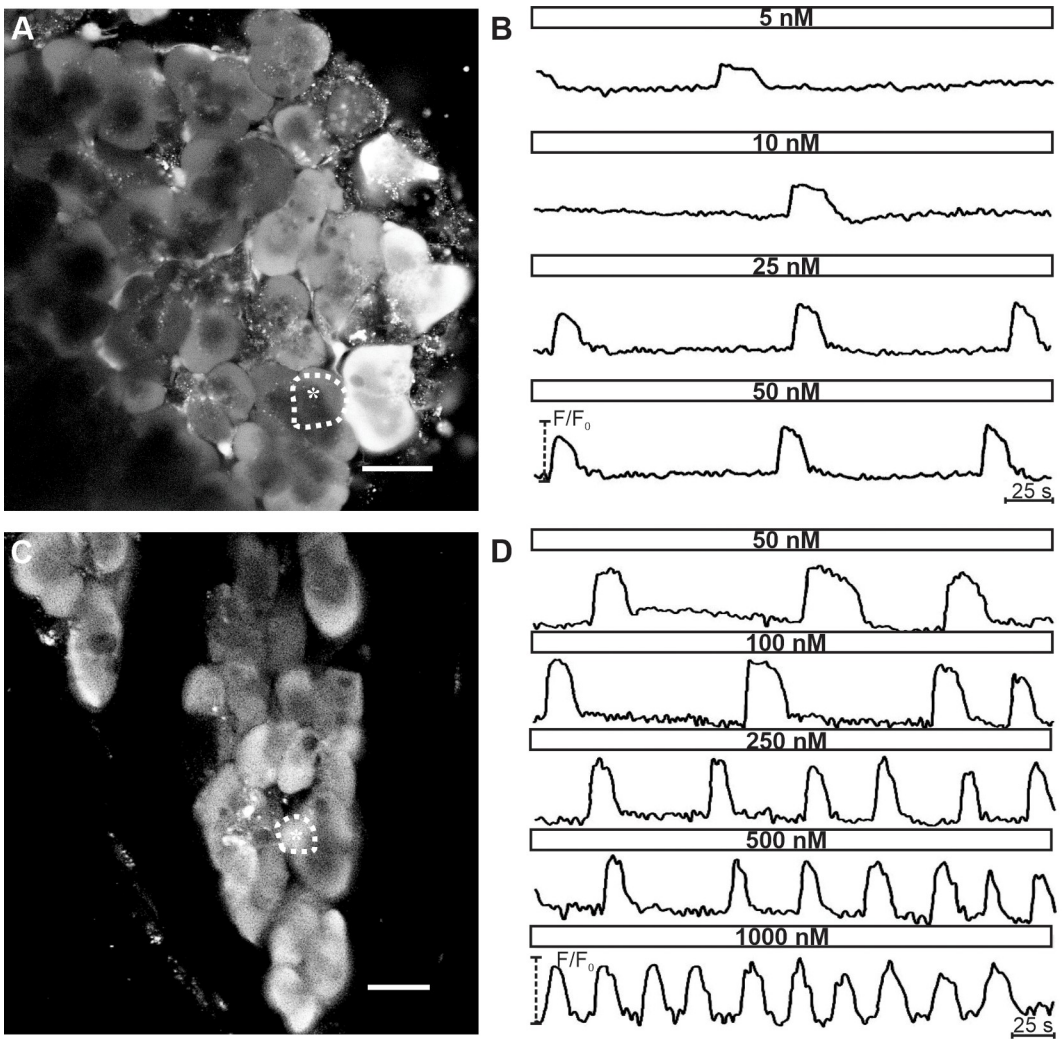

Fig 5. $[Ca^{2+}]_i$ oscillations in acinar cells stimulated with ACh display concentration-dependence. (A) and (C) OGB-1 loaded acinar cells in a tissue slice. Scale bar in Fig 5A 10 μm and in Fig 5C 20 μm. (B) $[Ca^{2+}]_i$ oscillations in an acinar cell in response to ACh concentrations ranging from 5 to 50 nM. The corresponding acinar cell is marked with thin broken line and asterisk in (A). (D) $[Ca^{2+}]_i$ oscillations cell in an acinar cell in response to ACh concentrations ranging from 50 to 1000 nM. The corresponding acinar cell is marked with thin broken line and asterisk in (C).

https://doi.org/10.1371/journal.pone.0268644.g005

results showing the average intra-acinar coactivity for different ACh concentrations are presented in Fig 7D. We could not detect statistically significant differences in respect to ACh concentration, most probably due to large inter-acinar and inter-slice variability. In an attempt to overcome this issue, we again present pooled data for low (5–25 nM), intermediate (50–100 nM), and high (250–1000 nM) ACh concentration in Fig 7E, similar to Fig 6. The average coactivity coefficient between different cells within acini had a median value 0.64 in the low concentration range that increased to a significantly higher median value of 0.73 in the high concentration range.

Dose-dependent $[Ca^{2+}]_i$ responses to cerulein

To test whether acinar cells in slices also respond to cerulein, a decapeptide cholecystokinin receptor agonist, and to compare its effect on $[Ca^{2+}]_i$ oscillations with responses to ACh, we

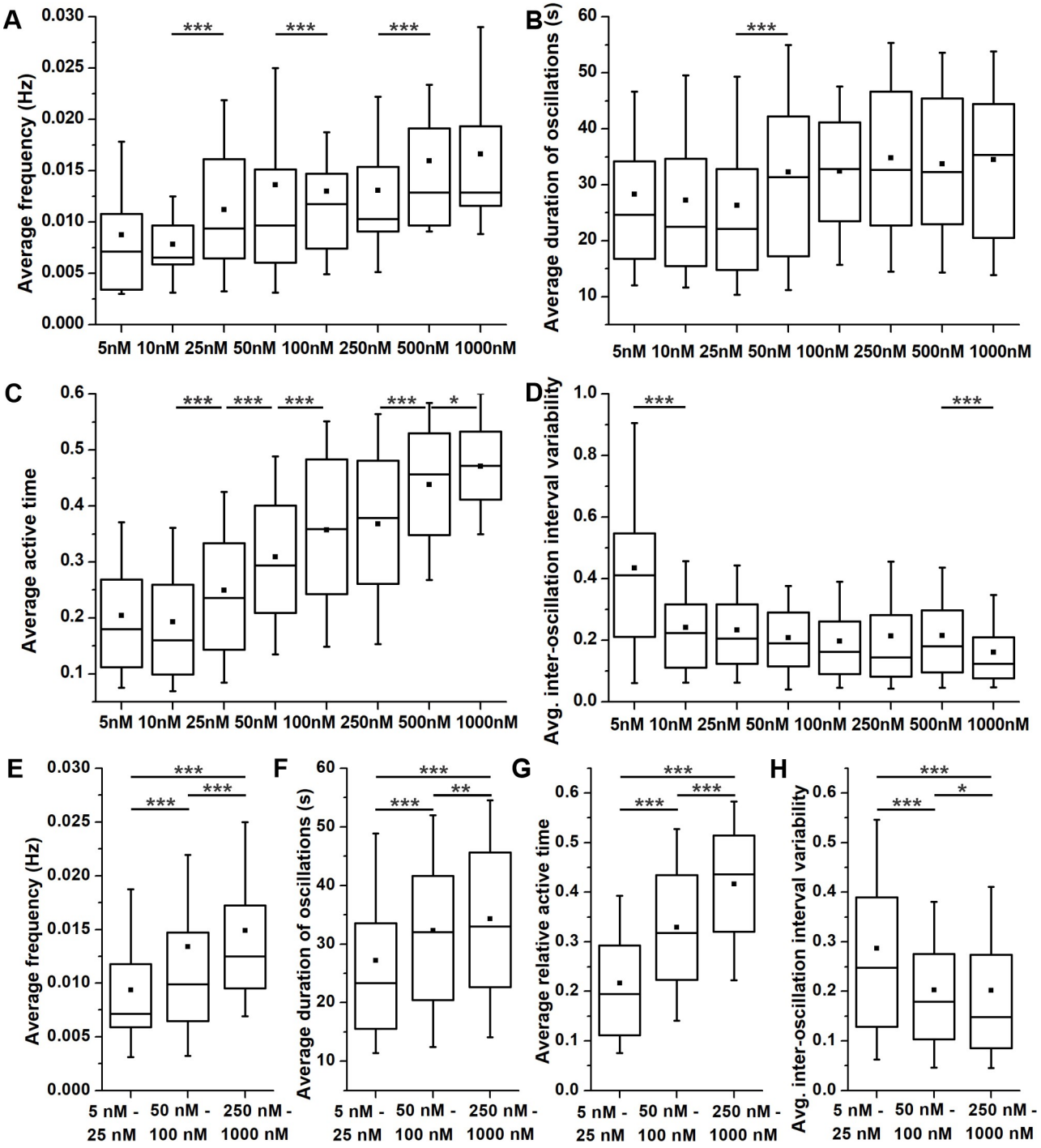

Fig 6. The dose-dependence of $[Ca^{2+}]_i$ oscillations in acinar cells upon stimulation with different concentrations of ACh. (A) and (E) Average frequency of oscillations. (B) and (F) Average duration of oscillations. (C) and (G) Average relative active time of oscillations. (D) and (H) Average inter-oscillation interval variability. Boxes determinate the interval within the 25th and the 75th percentile, whiskers denote the minimal and the maximal values, lines within the boxes indicate the median, and small squares stand for the average value. Significant differences are indicted by asterisks (*, $p<0.05$; **, $p<0.01$; ***, $p<0.001$). Panels E-H present pooled data for low (5–25 nM), medium (50–100 nM), and high (250–1000 nM) ACh concentrations. Number of analyzed slices/cells: 12/177 at 5 nM; 11/195 at 10 nM; 12/212 at 25 nM; 24/506 at 50 nM; 14/362 at 100 nM; 13/358 at 250 nM; 11/310 at 500 nM and 6/191cells at 1000 nM.

https://doi.org/10.1371/journal.pone.0268644.g006

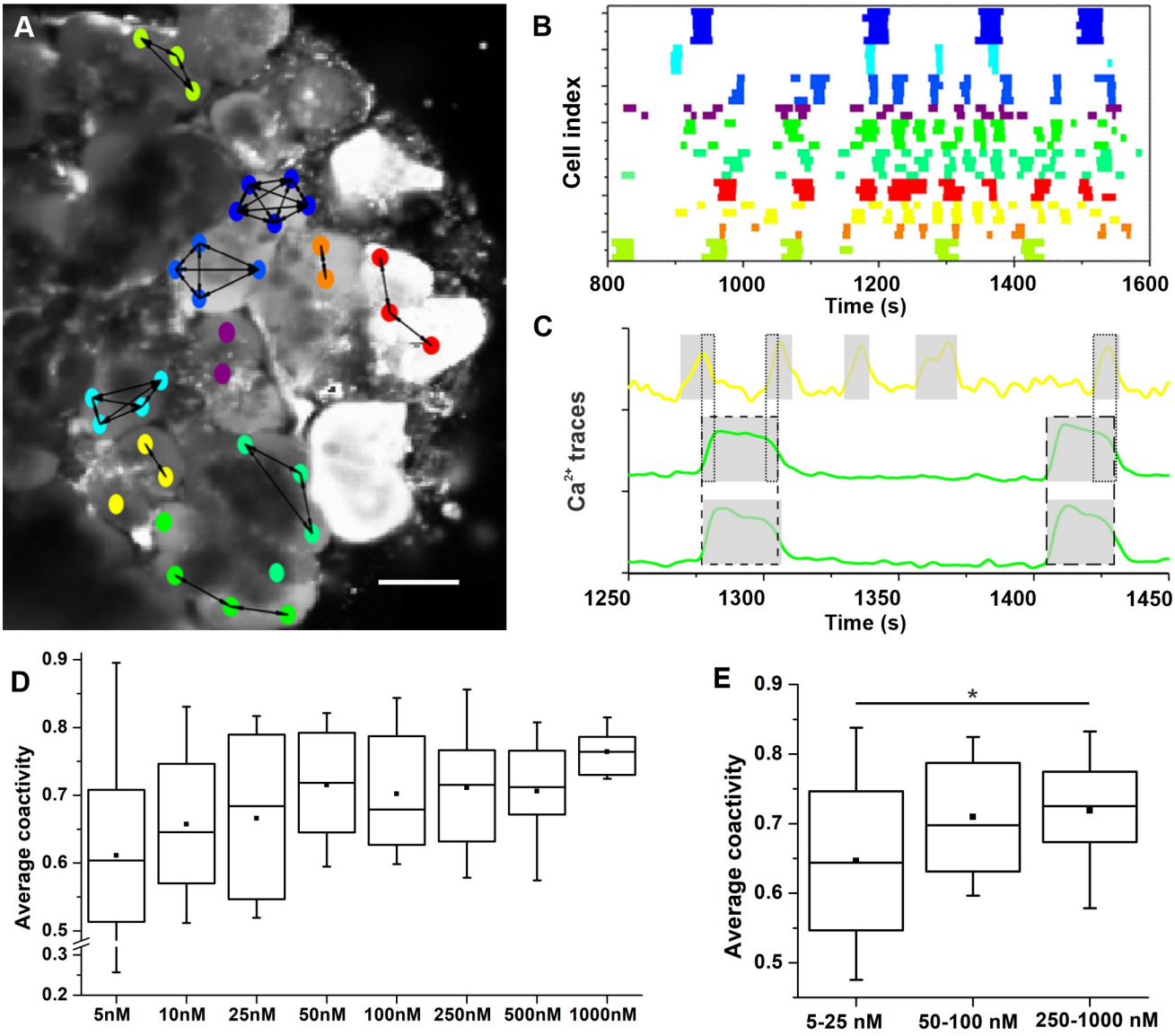

Fig 7. Inter-cellular synchronization of acinar cells. (A) Functional network of acinar cells extracted from coactivity and overlayed over a corresponding confocal image. Nodes denote individual acinar cells, colors code individual acini (matching the colors in panel B), and connections represent functional associations between synchronized cells, i.e., connections were established if the coactivity coefficient exceeded 0.65). Scale bar 10 μm. (B) Raster plot of binarized activity of all acinar cells in the field of view of a tissue slice during stimulation with 50 nM ACh. White color indicates no activity, other colors represent states with elevated $[Ca^{2+}]_i$ in particular cells, whereby colors denote individual acini. (C) Visualized coactivity between three different cells, whereby two of them were located in the same acinus (green line) and the third cell belonged to a separate acinus (yellow). The grey shaded areas indicate the duration of $[Ca^{2+}]_i$ oscillations of individual cells and the dashed and dotted lines the degree of coactivity (i.e., overlap in activity) between the two cells displayed in green and the middle green and yellow cell, respectively. (D) Dose-dependent average coactivity between acinar cells within individual acini. (E) Pooled data for low (5–25 nM), medium (50–100 nM), and high (250–1000 nM) ACh concentrations. Boxes determinate the interval within the 25th and the 75th percentile, whiskers denote the minimal and the maximal values, lines within the boxes indicate the median and small squares stand for the average value. Significant difference is indicted by asterisk (*, $p<0.05$).

https://doi.org/10.1371/journal.pone.0268644.g007

stimulated slices with cerulein at a 10 pM, 100 pM and 1000 pM concentration, as employed before [59]. The results are presented in Fig 8. After applying cerulein, a latent period of 90-120s was observed before cells reacted to secretagogue and entered the phase of a stable oscillatory activity. The oscillations after simulation with 10 pM cerulein and 100 pM cerulein were the result of repetitive, semiregular cycles of elevated and subsequently decreasing $[Ca^{2+}]_i$

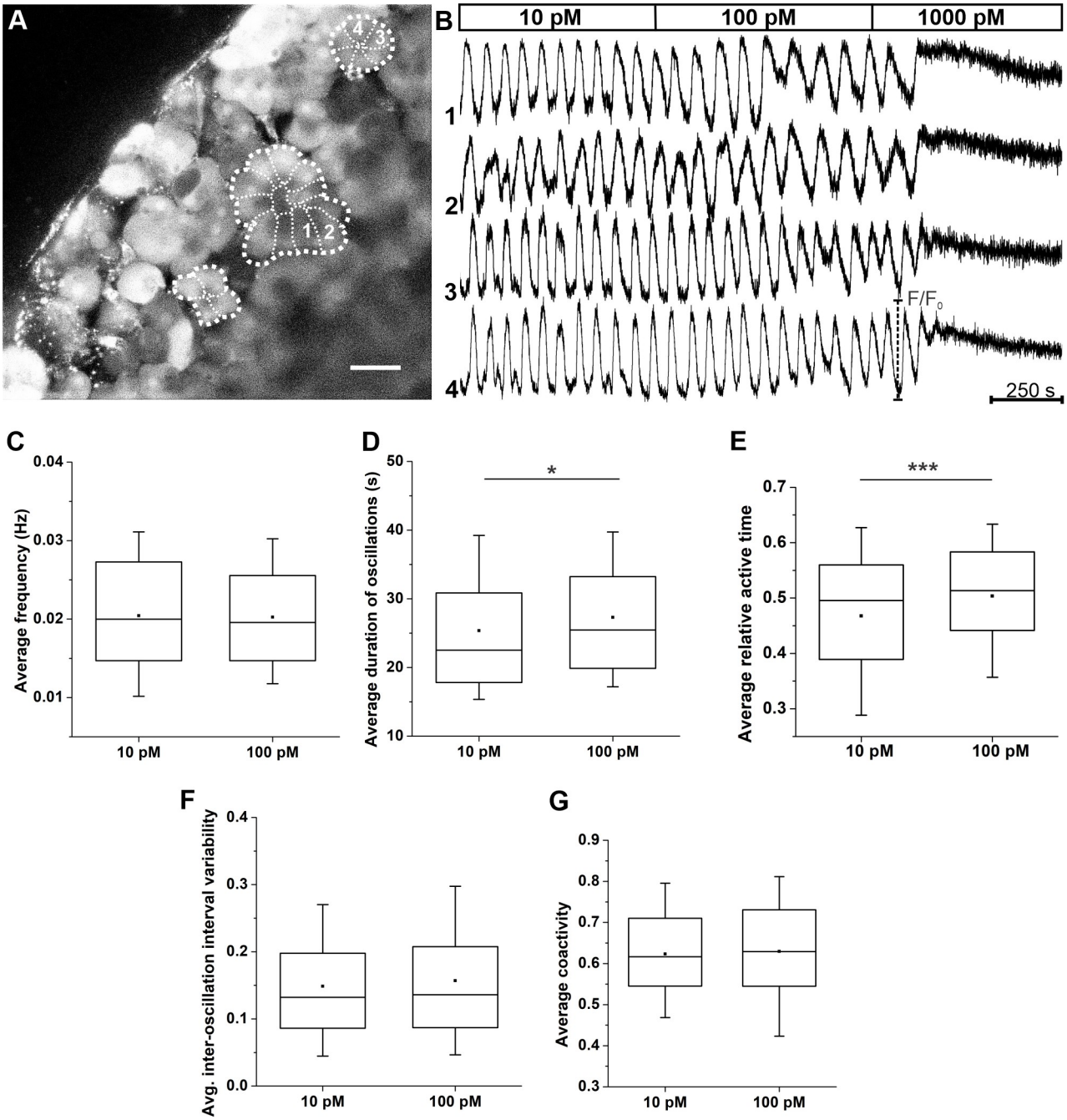

Fig 8. Activity of acinar cells during stimulation with cerulein. (A) Acinar cells loaded with the calcium dye. Cells indicated with 1 and 2 belong to a different acinus as cells 3 and 4 (the thicker broken line marks the acinus, the thinner broken lines mark boundaries between individual acinar cells). (B) Acinar cell activity during stimulation with increasing cerulein concentrations. Shown are four traces from two different acini, as indicated in panel A. (C) Average oscillation frequency. (D) Average oscillation duration. (E) Average relative active time. (F) Average inter-oscillation interval variability. (G) Average coactivity (G). Number of analyzed slices/cells 11/606 at 10 pM CCK and 11/571 at 100 pM CCK.

https://doi.org/10.1371/journal.pone.0268644.g008

levels (Fig 8B), similarly to what was reported before [25, 91, 93, 94]. The observed oscillations were similar in the same acinus, but typically differed between acini, analogous to what we observed in the case of ACh (Fig 4). Stimulation of pancreatic acinar cells with 1000 pM cerulein evoked a biphasic increase in basal $[Ca^{2+}]_i$ concentration, i.e., a peak and a plateau phase,

whereby the latter was characterized by a tonic and non-oscillatory increase in $[Ca^{2+}]_i$. A quantitative analysis revealed a dose-dependent $[Ca^{2+}]_i$ response to cerulein. We analyzed the activity only at 10 pM and 100 pM concentration, since the oscillations were saturated at 1000 pM (i.e., the active time amounted to unity or 100% in this case). The oscillatory activity at these two cerulein concentrations was rather high and comparable to responses detected at 500 nM or 1000 nM ACh (Fig 6). Moreover, we observed a significant increase of the duration of oscillations and relative active time at higher cerulein concentrations (Fig 8D and 8E). In contrast, the frequency of oscillations (Fig 8C), their regularity (Fig 8F), and the degree of inter-cellular synchronization (Fig 8G) were not found to be concentration-dependent.

Discussion

Understanding normal and pathological pancreas morphology and physiology is important due to diseases that affect this bifunctional gland. The tissue slice approach has established itself as an instrumental experimental approach in the past two decades, representing a cornerstone of studies on the structure and function of endocrine [58, 62–64, 70], ductal [65], and acinar cells [50, 59, 66, 67, 74, 95]. In our previous work, we have shown that the tissue slice methodology does not critically alter the morphology and function of the islets of Langerhans and ductal cells [61, 65, 70, 96]. By using a combination of morphological and functional assessments, including confocal live-cell $[Ca^{2+}]_i$ imaging in the present study, we further demonstrate that the acinar cells also remain morphologically and functionally intact in tissue slices, making them an attractive future approach to study acinar cells and their association with ductal and endocrine cells. More specifically, our morphological assessments show that the viability, structure, and ultrastructure of acinar cells and their organization into acini remain largely intact in acute tissue slices, corroborating the few previous reports in mouse [50, 59] and human tissue slices [66, 67, 97].

From the functional point of view, ACh and CCK are potent triggers for the stimulus secretion cascade (SSC) that results in secretion of enzymes. Previous studies demonstrated that acinar cells respond to these agonists with $[Ca^{2+}]_i$ oscillations, but with different temporal patterns [91, 98, 99], that there is typically a delay between the $[Ca^{2+}]_i$ increase in the apical and the basal pole (S1 Fig) [25], and that high concentrations induce a biphasic response lacking oscillations [90, 100–102]. Scarce and partially conflicting data are available on how acinar cells transduce differences in ACh and CCK concentration into differences in $[Ca^{2+}]_i$. A threshold concentration of 1 μM ACh and 1 nM CCK induced an oscillatory response [73, 93, 103], while others reported a biphasic response even at concentrations below 1 μM or 1 nM [91, 99, 104]. Since only a few studies reported a dose-dependent change in either frequency or duration of oscillations, we understand the ACh and CCK encoding only partially [73, 91, 99]. Other indices of the coding properties came from the optical study of zymogen granule dynamics, demonstrating two distinct pools of vesicles [105]. A threshold ACh concentration of 10–50 nM activated a subpopulation of vesicles with high fusion rates, followed by recruitment of slowly releasable granules, consistent with the biphasic profile of enzyme secretion from acinar cells [12, 105–108]. While above-threshold ACh concentrations (250 nM—10 μM) increased the overall vesicle fusion rate in a dose-dependent manner, the effect was limited to the slowly releasable pool. In sum, it seems that the ACh response is modulated in at least two steps along the SCC cascade, changing both the calcium dynamics and vesicle recruitment independently. However, this view is further complicated by the oscillatory nature of the calcium response to ACh that was neglected by studies on granule dynamics.

The previous inconsistent data on the acinar cell response to different ACh concentrations were the primary motivation for our study. In our hands, acinar cells responded to ACh

stimulation with repetitive $[Ca^{2+}]_i$ oscillations up to 1000 nM (Figs 3 and 5) and for the CCK receptor agonist cerulein up to 100 pM (Fig 8B). Applying a stimulation protocol consisting of a step-wise increase in ACh concentration from physiological to supraphysiological concentrations, we demonstrated that an increase in ACh stimulation increased both the frequency and the duration of the oscillations (Fig 6). We observed a 139% increase in both the duration and the frequency in the intermediate ACh concentration range (up to 100 nM), indicating that the coding of ACh concentrations employs both parameters equally. Higher ACh concentrations affected the acinar cells less (3–27%, Fig 6), consistent with a saturation of ACh response. Others reported that ACh, used in the range of 10–500 nM, evoked similar durations [73, 91, 99, 109], but surprisingly high frequencies (0.05–0.13 Hz), a whole order of magnitude faster than in our hands [90, 91, 94], a finding that deserves to be addressed in future studies. In experiments with cerulein, we observed an increase in duration and relative active time, when comparing physiological (10 pM) and submaximal (100 pM) concentrations. The calculated frequency and duration were 0.02 Hz and 23 s at lower cerulein values, which is consistent with previous reports [91, 93, 99, 109]. Furthermore, Tsunoda et al. reported a decrease in frequency and amplitude with higher CCK values although the peak of $[Ca^{2+}]_i$ was observed at 1 nM CCK, which is also consistent with our findings. This observed decrease is probably related to the large initial increase in $[Ca^{2+}]_i$ after low CCK stimulations [93].

At least two alternative ACh-coding mechanisms were proposed in other tissues. On the one hand, ACh-dependent recruitment of oscillating cells was reported in airway smooth muscle cells [110, 111] and in pancreatic beta cells [112]. CCK-dependent recruitment of oscillating cells was also reported in pancreatic acinar cells in terms of receptor-mediated $[Ca^{2+}]_i$ mobilization [113]. On the other hand, amplitude modulation was observed in cortical neurons [114], and this mechanism is most probably not involved in acinar cells [105].

Spontaneous $[Ca^{2+}]_i$ oscillations were observed in our study in about half of the cells. It has been reported that $[Ca^{2+}]_i$ oscillations in non-excitable cells, such as pancreatic acinar cells, can be preceded by a gradual increase in $[Ca^{2+}]_i$ that resembles a pacemaker potential. This phenomenon was first observed in endothelial cells and hepatocytes [115–117], and later, in mesenchymal stem cells [118, 119] and salivary gland ductal cells [120], and is believed to be linked to IP_3R activation and Ca^{2+} influx, as well as an ATP-mediated autocrine/paracrine signaling pathway [121–124]. The spontaneous oscillations clearly require further attention in future studies to explain their mechanistic substrate. Since they have been described in other tissues and were present immediately at the beginning of the recording in our study, they probably represent a true biological phenomenon and were not caused by phototoxicity or excess laser exposure of cells loaded with fluorophores [125].

The $[Ca^{2+}]_i$ increases generated through agonist stimulation are not exclusively limited to a single acinar cell but can also propagate from one cell to another. Inter-cellular coupling between acinar cells by gap junctions consisting of Cx32 and Cx26 makes it possible for the Ca^{2+} signals to travel in a wave-like manner between the cells and thereby serve as a means of inter-cellular communication [30]. This leads to a rather coordinated and higher $[Ca^{2+}]_i$ activity of acinar cells when compared to isolated cells and has been suggested to affect digestive enzyme secretion [24, 29]. Alternatively, signal transmission can be facilitated by ATP release into the extracellular space or stretch-activated Ca^{2+} channels [126]. Moreover, it has been reported that stimulation with high ACh concentrations or other cholinergic analogs leads to a partial uncoupling of pancreatic acinar cells. The non-trivial modulation of gap junctional coupling between acinar cells is thought to be a crucial determinant of initiating, maintaining, or enhancing the increased secretion of pancreatic enzymes [26, 127]. Our analysis did not observe a drop in coordinated Ca^{2+} activity at the highest employed stimulation levels but a slight increase in synchronicity. However, it should be noted that our evaluation of

synchronous behavior in acinar cells *in situ* does not directly reflect the extent of gap-junctional coupling only but also encompasses the overall activity and regularity of oscillations, both of which seem to increase with increasing levels of ACh (Fig 6), which was not the case for cerulein (Fig 8). Particularly under low concentrations of agonists, there appears to be a higher degree of fluctuations in oscillation periods, as under these circumstances, the $[Ca^{2+}]_i$ activity is more prone to stochasticity due to random opening and closing of Ca^{2+} channels [74, 128, 129]. Furthermore, our results coincide with previous reports showing that the acinar cells are well connected within acini and not between acini. More specifically, in functional cellular networks constructed from $[Ca^{2+}]_i$ activity, a well-stablished methodology to evaluate inter-cellular connectivity patterns [82], connections were established solely between cells from the same acini (Fig 7A). Therefore, in the future, such a functional assessment could in principle be used to help discriminate acinar cells and different acini within tissue slices and supplement the characterization based on morphological data [130, 131]. Finally, despite the rather well-aligned $[Ca^{2+}]_i$ oscillations within individual acini, the patterns of inter-cellular activity appear to be quite erratic and without a clear course. This is most probably related to the functional and morphological polarity, stochastic influences, and various $[Ca^{2+}]_i$ handling mechanisms in acinar cells. Namely, computational models that have been developed to elucidate the processes governing the inter-cellular $[Ca^{2+}]_i$ dynamics have shown that spatially distributed diffusion and cell geometry both play important roles in determining behavior in pancreatic acinar cells [132, 133]. Most importantly, this also strongly impacts inter-cellular activity and synchronization of oscillations between cells and results in a variety of synchronous, phase-locked, or even asynchronous behaviors [134], similar to what we observed in our experiments. To investigate these issues in further detail, we encourage additional experimental studies as well as the development of multicellular models that would incorporate acinar cell structure and heterogeneity along with the temporal and agonist-dependent variability of gap-junctional conductance. This would enable a more holistic assessment of the complex and variable $[Ca^{2+}]_i$ activity patterns in pancreatic acini.

To conclude, animal models of disease in combination with the acute pancreas tissue slice have been used to assess morphological changes and elucidate the background etiopathogenesis of common pancreatic disorders such as type 2 diabetes in chemically induced [64] or genetic models [135]. This methodology offers background for the use of more contemporary models of disease like Western diet induced type 2 diabetes [136] and acute pancreatitis [137] with the tissue slice technique. With the adaptation of the tissue slice technique for human and porcine tissue [50, 138, 139], findings are more suitable for application to human (patho)physiology, and the disadvantages of animal experiments can be omitted. Finally, inspiring approaches, such as the syncollin-pHluorin construct delivered by adenovirus transfection [140], and extracellular dyes that transiently enter the vesicles while in the fused state [141–143], would allow the study of spatiotemporal vesicle dynamics in a large number of acinar cells simultaneously. This approach could help explain whether calcium dynamics suffice to elucidate the vesicle fusion properties [67, 144] in health and disease and help pinpoint novel pharmacological targets [35, 145].

Supporting information

S1 Fig. $[Ca^{2+}]_i$ activity within a single acinar cell. (A) Acinar cells loaded with the calcium reporter dye. (B) Morphological visualization of an acinus using scanning gradient contrast (Dodt) imaging. Cell boundaries and temporal differences in signals between cells visible on calcium imaging (A), and cell boundaries and granules on apical poles visible on Dodt imaging (B) were used to identify an acinus and individual cells. Scale bar 10 μm. (C) $[Ca^{2+}]_i$ activity of

acinar cells that were identified from calcium imaging (A) and Dodt imaging (B) to have a common orientation of the apical poles. Acinar cells are depicted and numbered. The blue and red dot indicate parts of the basal and apical pole, referred to in (E). (D) $[Ca^{2+}]_i$ oscillatory activity in numbered acinar cells after stimulation with 500 nM ACh. (E) $[Ca^{2+}]_i$ oscillatory activity from apical (blue) and basal (red) pole of the acinar cell (C) during stimulation with 500 nM ACh. Note the apical-to-basal temporal delay in $[Ca^{2+}]_i$ increase.
(TIF)

S2 Fig. Comparison between fluorescent $[Ca^{2+}]_i$ indicators Oregon Green BAPTA-1 (OGB-1) and Calbryte 520 AM. $[Ca^{2+}]_i$ oscillations after stimulation with 100nM ACh loaded with OGB-1 (A) and Calbryte 520 AM (B). Comparison between the measured relative active times (C) and the average inter-oscillation interval variability (D) using different dyes.
(TIF)

S3 Fig. Quantification of cell viability in the tissue slice preparation. A Montage of a z-stack following LIVE/DEAD double staining. Individual panels depict different focal plains (indicated with numbers). Green color indicates live cells labeled with calcein-AM and red color indicates dead cells labeled with EthD-1. Scale bar 50 μm.
(TIF)

Acknowledgments

The authors thank Rudi Mlakar and Maruša Rošer for excellent technical support and Lidija Križančić Bombek and Maša Skelin Klemen for help with experimental work. In addition, we want to appreciate the support of the chief of the Clinical Department of Abdominal and General Surgery, University Medical Centre Maribor, prof. Stojan Potrč, MD, PhD and all the other colleagues from the department.

Author Contributions

Conceptualization: Urška Marolt, Jurij Dolenšek, Andraž Stožer.

Data curation: Urška Marolt, Eva Paradiž Leitgeb, Viljem Pohorec, Saška Lipovšek, Viktória Venglovecz, Eleonóra Gál, Attila Ébert, István Menyhárt, Jurij Dolenšek, Andraž Stožer.

Formal analysis: Urška Marolt, Eva Paradiž Leitgeb, Viljem Pohorec, Saška Lipovšek, Viktória Venglovecz, Eleonóra Gál, Marko Gosak.

Funding acquisition: Urška Marolt.

Investigation: Urška Marolt.

Methodology: Viktória Venglovecz, Attila Ébert, István Menyhárt, Marko Gosak, Jurij Dolenšek, Andraž Stožer.

Project administration: Stojan Potrč, Jurij Dolenšek, Andraž Stožer.

Resources: Stojan Potrč, Andraž Stožer.

Software: Marko Gosak.

Supervision: Stojan Potrč, Jurij Dolenšek, Andraž Stožer.

Validation: Jurij Dolenšek, Andraž Stožer.

Writing – original draft: Urška Marolt, Eva Paradiž Leitgeb, Viljem Pohorec, Attila Ébert, Marko Gosak, Jurij Dolenšek, Andraž Stožer.

Writing – review & editing: Eva Paradiž Leitgeb, Viljem Pohorec, Saška Lipovšek, Viktória Venglovecz, Eleonóra Gál, Stojan Potrč, Marko Gosak, Jurij Dolenšek, Andraž Stožer.

References

1. Parys JB, Bultynck G. Calcium signaling in health, disease and therapy. Biochim Biophys Acta Mol Cell Res. 2018; 1865: 1657–1659. https://doi.org/10.1016/j.bbamcr.2018.08.019 PMID: 30798945
2. Roberts SE, Morrison-Rees S, John A, Williams JG, Brown TH, Samuel DG. The incidence and aetiology of acute pancreatitis across Europe. Pancreatol Off J Int Assoc Pancreatol IAP Al. 2017; 17: 155–165. https://doi.org/10.1016/j.pan.2017.01.005 PMID: 28159463
3. Forouhi NG, Wareham NJ. Epidemiology of diabetes. Med Abingdon Engl UK Ed. 2014; 42: 698–702. https://doi.org/10.1016/j.mpmed.2014.09.007 PMID: 25568613
4. Khalaf N, El-Serag HB, Abrams HR, Thrift AP. Burden of Pancreatic Cancer: From Epidemiology to Practice. Clin Gastroenterol Hepatol Off Clin Pract J Am Gastroenterol Assoc. 2020. https://doi.org/10.1016/j.cgh.2020.02.054 PMID: 32147593
5. Leung PS. Common pancreatic disease. Adv Exp Med Biol. 2010; 690: 29–51. https://doi.org/10.1007/978-90-481-9060-7_3 PMID: 20700836
6. Barreto SG, Habtezion A, Gukovskaya A, Lugea A, Jeon C, Yadav D, et al. Critical thresholds: key to unlocking the door to the prevention and specific treatments for acute pancreatitis. Gut. 2021; 70: 194–203. https://doi.org/10.1136/gutjnl-2020-322163 PMID: 32973069
7. Dolenšek J, Rupnik MS, Stožer A. Structural similarities and differences between the human and the mouse pancreas. Islets. 2015; 7. https://doi.org/10.1080/19382014.2015.1024405 PMID: 26030186
8. Weiss FU, Halangk W, Lerch MM. New advances in pancreatic cell physiology and pathophysiology. Best Pract Res Clin Gastroenterol. 2008; 22: 3–15. https://doi.org/10.1016/j.bpg.2007.10.017 PMID: 18206809
9. McGuckin E, Cade JE, Hanison J. The pancreas. Anaesth Intensive Care Med. 2020; 21: 604–610. https://doi.org/10.1016/j.mpaic.2020.08.005
10. Dolenšek J, Pohorec V, Slak Rupnik M, Stožer A. Pancreas Physiology. Challenges in Pancreatic Pathology. IntechOpen; 2017. https://doi.org/10.5772/65895
11. Gerich JE. Physiology of glucose homeostasis. Diabetes Obes Metab. 2000; 2: 345–350. https://doi.org/10.1046/j.1463-1326.2000.00085.x PMID: 11225963
12. Low JT, Shukla A, Thorn P. Pancreatic acinar cell: new insights into the control of secretion. Int J Biochem Cell Biol. 2010; 42: 1586–1589. https://doi.org/10.1016/j.biocel.2010.07.006 PMID: 20637893
13. Pandiri AR. Overview of exocrine pancreatic pathobiology. Toxicol Pathol. 2014; 42: 207–216. https://doi.org/10.1177/0192623313509907 PMID: 24190915
14. Petersen OH. Stimulus-secretion coupling: cytoplasmic calcium signals and the control of ion channels in exocrine acinar cells. J Physiol. 1992; 448: 1–51. https://doi.org/10.1113/jphysiol.1992.sp019028 PMID: 1375633
15. Williams JA. Receptor-mediated signal transduction pathways and the regulation of pancreatic acinar cell function. Curr Opin Gastroenterol. 2008; 24: 573–579. https://doi.org/10.1097/MOG.0b013e32830b110c PMID: 19122497
16. Almaça J, Caicedo A, Landsman L. Beta cell dysfunction in diabetes: the islet microenvironment as an unusual suspect. Diabetologia. 2020; 63: 2076–2085. https://doi.org/10.1007/s00125-020-05186-5 PMID: 32894318
17. Panzer JK, Hiller H, Cohrs CM, Almaça J, Enos SJ, Beery M, et al. Pancreas tissue slices from organ donors enable in situ analysis of type 1 diabetes pathogenesis. JCI Insight. 2020; 5. https://doi.org/10.1172/jci.insight.134525 PMID: 32324170
18. Eberhard D, Kragl M, Lammert E. "Giving and taking": endothelial and beta-cells in the islets of Langerhans. Trends Endocrinol Metab TEM. 2010; 21: 457–463. https://doi.org/10.1016/j.tem.2010.03.003 PMID: 20359908
19. Bläuer M, Nordback I, Sand J, Laukkarinen J. A novel explant outgrowth culture model for mouse pancreatic acinar cells with long-term maintenance of secretory phenotype. Eur J Cell Biol. 2011; 90: 1052–1060. https://doi.org/10.1016/j.ejcb.2011.07.004 PMID: 21906833
20. Manuel Cancela J, Gerasimenko OV, Gerasimenko JV, Tepikin AV, Petersen OH. Two different but converging messenger pathways to intracellular Ca2+ release: the roles of nicotinic acid adenine dinucleotide phosphate, cyclic ADP-ribose and inositol trisphosphate. EMBO J. 2000; 19: 2549–2557. https://doi.org/10.1093/emboj/19.11.2549 PMID: 10835353

21. Petersen CC, Toescu EC, Petersen OH. Different patterns of receptor-activated cytoplasmic Ca2+ oscillations in single pancreatic acinar cells: dependence on receptor type, agonist concentration and intracellular Ca2+ buffering. EMBO J. 1991; 10: 527–533. https://doi.org/10.1002/j.1460-2075.1991.tb07979.x PMID: 1705883

22. Petersen OH, Tepikin AV. Polarized calcium signaling in exocrine gland cells. Annu Rev Physiol. 2008; 70: 273–299. https://doi.org/10.1146/annurev.physiol.70.113006.100618 PMID: 17850212

23. Thorn P, Gaisano H. Molecular control of compound Exocytosis. Commun Integr Biol. 2012; 5: 61–63. https://doi.org/10.4161/cib.18058 PMID: 22482012

24. Yule DI, Stuenkel E, Williams JA. Intercellular calcium waves in rat pancreatic acini: mechanism of transmission. Am J Physiol. 1996; 271: C1285–1294. https://doi.org/10.1152/ajpcell.1996.271.4.C1285 PMID: 8897836

25. Thorn P, Lawrie AM, Smith PM, Gallacher DV, Petersen OH. Local and global cytosolic Ca2+ oscillations in exocrine cells evoked by agonists and inositol trisphosphate. Cell. 1993; 74: 661–668. https://doi.org/10.1016/0092-8674(93)90513-p PMID: 8395347

26. Chanson M, Mollard P, Meda P, Suter S, Jongsma HJ. Modulation of Pancreatic Acinar Cell to Cell Coupling during ACh-evoked Changes in Cytosolic Ca2+. J Biol Chem. 1999; 274: 282–287. https://doi.org/10.1074/jbc.274.1.282 PMID: 9867842

27. Peterson OH, Iwatsuki N. The role of calcium in pancreatic acinar cell stimulus-secretion coupling: an electrophysiological approach. Ann N Y Acad Sci. 1978; 307: 599–617. https://doi.org/10.1111/j.1749-6632.1978.tb41984.x PMID: 360950

28. Meda P. Gap junction involvement in secretion: the pancreas experience. Clin Exp Pharmacol Physiol. 1996; 23: 1053–1057. https://doi.org/10.1111/j.1440-1681.1996.tb01168.x PMID: 8977159

29. Stauffer PL, Zhao H, Luby-Phelps K, Moss RL, Star RA, Muallem S. Gap junction communication modulates [Ca2+]i oscillations and enzyme secretion in pancreatic acini. J Biol Chem. 1993; 268: 19769–19775. PMID: 8366115

30. Cigliola V, Allagnat F, Berchtold LA, Lamprianou S, Haefliger J-A, Meda P. Role of Connexins and Pannexins in the Pancreas. Pancreas. 2015; 44: 1234–1244. https://doi.org/10.1097/MPA.0000000000000378 PMID: 26465951

31. Gerasimenko JV, Gerasimenko OV, Petersen OH. The role of Ca2+ in the pathophysiology of pancreatitis. J Physiol. 2014; 592: 269–280. https://doi.org/10.1113/jphysiol.2013.261784 PMID: 23897234

32. Li J, Zhou R, Zhang J, Li Z-F. Calcium signaling of pancreatic acinar cells in the pathogenesis of pancreatitis. World J Gastroenterol WJG. 2014; 20: 16146–16152. https://doi.org/10.3748/wjg.v20.i43.16146 PMID: 25473167

33. Raraty MGT, Murphy JA, McLoughlin E, Smith D, Criddle D, Sutton R. Mechanisms of Acinar Cell Injury in Acute Pancreatitis. Scand J Surg. 2005; 94: 89–96. https://doi.org/10.1177/145749690509400202 PMID: 16111088

34. Pallagi P, Madácsy T, Varga Á, Maléth J. Intracellular Ca2+ Signalling in the Pathogenesis of Acute Pancreatitis: Recent Advances and Translational Perspectives. Int J Mol Sci. 2020; 21. https://doi.org/10.3390/ijms21114005 PMID: 32503336

35. Petersen OH, Gerasimenko JV, Gerasimenko OV, Gryshchenko O, Peng S. The roles of calcium and ATP in the physiology and pathology of the exocrine pancreas. Physiol Rev. 2021; 101: 1691–1744. https://doi.org/10.1152/physrev.00003.2021 PMID: 33949875

36. Morisset J. Seventy years of pancreatic physiology: take a look back. Pancreas. 2014; 43: 1172–1184. https://doi.org/10.1097/MPA.0000000000000226 PMID: 25333400

37. Williams JA, Korc M, Dormer RL. Action of secretagogues on a new preparation of functionally intact, isolated pancreatic acini. Am J Physiol. 1978; 235: 517–524. https://doi.org/10.1152/ajpendo.1978.235.5.E517 PMID: 215042

38. Blinman TA, Gukovsky I, Mouria M, Zaninovic V, Livingston E, Pandol SJ, et al. Activation of pancreatic acinar cells on isolation from tissue: cytokine upregulation via p38 MAP kinase. Am J Physiol Cell Physiol. 2000; 279: C1993–2003. https://doi.org/10.1152/ajpcell.2000.279.6.C1993 PMID: 11078716

39. Park MK, Lee M, Petersen OH. Morphological and functional changes of dissociated single pancreatic acinar cells: testing the suitability of the single cell as a model for exocytosis and calcium signaling. Cell Calcium. 2004; 35: 367–379. https://doi.org/10.1016/j.ceca.2003.10.003 PMID: 15036953

40. Ahn YB, Xu G, Marselli L, Toschi E, Sharma A, Bonner-Weir S, et al. Changes in gene expression in beta cells after islet isolation and transplantation using laser-capture microdissection. Diabetologia. 2007; 50: 334–342. https://doi.org/10.1007/s00125-006-0536-5 PMID: 17180350

41. Schmid A, Feick P, Schulz I. Inwardly rectifying, voltage-dependent and resting potassium currents in rat pancreatic acinar cells in primary culture. J Physiol. 1997; 504: 259–270. https://doi.org/10.1111/j.1469-7793.1997.259be.x PMID: 9365902

42. Amsterdam A, Jamieson JD. Studies on dispersed pancreatic exocrine cells. I. Dissociation technique and morphologic characteristics of separated cells. J Cell Biol. 1974; 63: 1037–1056. https://doi.org/10.1083/jcb.63.3.1037 PMID: 4373477

43. Amsterdam A, Jamieson JD. Studies on dispersed pancreatic exocrine cells. II. Functional characteristics of separated cells. J Cell Biol. 1974; 63: 1057–1073. https://doi.org/10.1083/jcb.63.3.1057 PMID: 4436379

44. Apte MV, Wilson JS. The importance of keeping in touch: regulation of cell-cell contact in the exocrine pancreas. Gut. 2005; 54: 1358–1359. https://doi.org/10.1136/gut.2005.070953 PMID: 16162948

45. Thorn P, Gaisano HY. Cell-to-Cell Communication and the Regulation of Pancreatic Function. Pancreas. 2015; 44: 1174–1175. https://doi.org/10.1097/MPA.0000000000000401 PMID: 26465945

46. de Vos P, Smink AM, Paredes G, Lakey JRT, Kuipers J, Giepmans BNG, et al. Enzymes for Pancreatic Islet Isolation Impact Chemokine-Production and Polarization of Insulin-Producing β-Cells with Reduced Functional Survival of Immunoisolated Rat Islet-Allografts as a Consequence. PloS One. 2016; 11: e0147992. https://doi.org/10.1371/journal.pone.0147992 PMID: 26824526

47. Zhao X, Han J, Tang C. Primary culture of porcine pancreatic acinar cells. JOP J Pancreas. 2001; 2: 78–82. PMID: 11867867

48. Bhagat L, Singh VP, Hietaranta AJ, Agrawal S, Steer ML, Saluja AK. Heat shock protein 70 prevents secretagogue-induced cell injury in the pancreas by preventing intracellular trypsinogen activation. J Clin Invest. 2000; 106: 81–89. https://doi.org/10.1172/JCI8706 PMID: 10880051

49. Lardon J, Bouwens L. Metaplasia in the pancreas. Differ Res Biol Divers. 2005; 73: 278–286. https://doi.org/10.1111/j.1432-0436.2005.00030.x PMID: 16138828

50. Marciniak A, Cohrs CM, Tsata V, Chouinard JA, Selck C, Stertmann J, et al. Using pancreas tissue slices for in situ studies of islet of Langerhans and acinar cell biology. Nat Protoc. 2014; 9: 2809–2822. https://doi.org/10.1038/nprot.2014.195 PMID: 25393778

51. Ballian N, Brunicardi FC. Islet vasculature as a regulator of endocrine pancreas function. World J Surg. 2007; 31: 705–714. https://doi.org/10.1007/s00268-006-0719-8 PMID: 17347899

52. Masamune A, Watanabe T, Kikuta K, Shimosegawa T. Roles of pancreatic stellate cells in pancreatic inflammation and fibrosis. Clin Gastroenterol Hepatol Off Clin Pract J Am Gastroenterol Assoc. 2009; 7: S48–54. https://doi.org/10.1016/j.cgh.2009.07.038 PMID: 19896099

53. Bertelli E, Bendayan M. Association between endocrine pancreas and ductal system. More than an epiphenomenon of endocrine differentiation and development? J Histochem Cytochem Off J Histochem Soc. 2005; 53: 1071–1086. https://doi.org/10.1369/jhc.5R6640.2005 PMID: 15956021

54. McIlwain H, Buddle HL. Techniques in tissue metabolism. 1. A mechanical chopper. Biochem J. 1953; 53: 412–420.2. https://doi.org/10.1042/bj0530412 PMID: 13032086

55. Skrede KK, Westgaard RH. The transverse hippocampal slice: a well-defined cortical structure maintained in vitro. Brain Res. 1971; 35: 589–593. https://doi.org/10.1016/0006-8993(71)90508-7 PMID: 5135556

56. de Boer TP, Camelliti P, Ravens U, Kohl P. Myocardial tissue slices: organotypic pseudo-2D models for cardiac research & development. Future Cardiol. 2009; 5: 425–430. https://doi.org/10.2217/fca.09.32 PMID: 19715406

57. Graaf IA de Groothuis GM, Olinga P. Precision-cut tissue slices as a tool to predict metabolism of novel drugs. Expert Opin Drug Metab Toxicol. 2007; 3: 879–898. https://doi.org/10.1517/17425255.3.6.879 PMID: 18028031

58. Speier S, Rupnik M. A novel approach to in situ characterization of pancreatic beta-cells. Pflugers Arch. 2003; 446: 553–558. https://doi.org/10.1007/s00424-003-1097-9 PMID: 12774232

59. Marciniak A, Selck C, Friedrich B, Speier S. Mouse pancreas tissue slice culture facilitates long-term studies of exocrine and endocrine cell physiology in situ. PloS One. 2013; 8: e78706. https://doi.org/10.1371/journal.pone.0078706 PMID: 24223842

60. Panzer JK, Cohrs CM, Speier S. Using Pancreas Tissue Slices for the Study of Islet Physiology. Methods Mol Biol Clifton NJ. 2020; 2128: 301–312. https://doi.org/10.1007/978-1-0716-0385-7_20 PMID: 32180201

61. Stožer A, Dolenšek J, Križančić Bombek L, Pohorec V, Slak Rupnik M, Skelin Klemen M. Confocal Laser Scanning Microscopy of Calcium Dynamics in Acute Mouse Pancreatic Tissue Slices. J Vis Exp JoVE. 2021. https://doi.org/10.3791/62293 PMID: 33938876

62. Speier S, Gjinovci A, Charollais A, Meda P, Rupnik M. Cx36-mediated coupling reduces beta-cell heterogeneity, confines the stimulating glucose concentration range, and affects insulin release kinetics. Diabetes. 2007; 56: 1078–1086. https://doi.org/10.2337/db06-0232 PMID: 17395748

63. Huang Y-C, Rupnik M, Gaisano HY. Unperturbed islet α-cell function examined in mouse pancreas tissue slices. J Physiol. 2011; 589: 395–408. https://doi.org/10.1113/jphysiol.2010.200345 PMID: 21078586

64. Huang Y-C, Slak Rupnik M, Karimian N, Herrera PL, Gilon P, Feng Z-P, et al. In situ electrophysiological examination of pancreatic α cells in the streptozotocin-induced diabetes model, revealing the cellular basis of glucagon hypersecretion. Diabetes. 2013; 62: 519–530. https://doi.org/10.2337/db11-0786 PMID: 23043159

65. Gál E, Dolenšek J, Stožer A, Pohorec V, Ébert A, Venglovecz V. A Novel in situ Approach to Studying Pancreatic Ducts in Mice. Front Physiol. 2019; 10. https://doi.org/10.3389/fphys.2019.00938 PMID: 31396104

66. Liang T, Dolai S, Xie L, Winter E, Orabi AI, Karimian N, et al. Ex vivo human pancreatic slice preparations offer a valuable model for studying pancreatic exocrine biology. J Biol Chem. 2017; 292: 5957–5969. https://doi.org/10.1074/jbc.M117.777433 PMID: 28242761

67. Dolai S, Liang T, Orabi AI, Holmyard D, Xie L, Greitzer-Antes D, et al. Pancreatitis-Induced Depletion of Syntaxin 2 Promotes Autophagy and Increases Basolateral Exocytosis. Gastroenterology. 2018; 154: 1805–1821.e5. https://doi.org/10.1053/j.gastro.2018.01.025 PMID: 29360461

68. Dolenšek J, Stožer A, Skelin Klemen M, Miller EW, Slak Rupnik M. The Relationship between Membrane Potential and Calcium Dynamics in Glucose-Stimulated Beta Cell Syncytium in Acute Mouse Pancreas Tissue Slices. PLoS ONE. 2013; 8. https://doi.org/10.1371/journal.pone.0082374 PMID: 24324777

69. Stožer A, Gosak M, Dolenšek J, Perc M, Marhl M, Slak Rupnik M, et al. Functional Connectivity in Islets of Langerhans from Mouse Pancreas Tissue Slices. PLoS Comput Biol. 2013; 9. https://doi.org/10.1371/journal.pcbi.1002923 PMID: 23468610

70. Stožer A, Dolenšek J, Slak Rupnik M. Glucose-stimulated calcium dynamics in islets of Langerhans in acute mouse pancreas tissue slices. PloS One. 2013; 8: e54638. https://doi.org/10.1371/journal.pone.0054638 PMID: 23358454

71. Stožer A, Dolenšek J, Skelin Klemen M, Slak Rupnik M. Cell Physiology in Tissue Slices Studying Beta Cells in the Islets of Langerhans. ACTA MEDICO–BIOTECHNICA. 2013: 20–32.

72. Wang L, Xie D, Wei D. Pancreatic Acinar-to-Ductal Metaplasia and Pancreatic Cancer. Methods Mol Biol Clifton NJ. 2019; 1882: 299–308. https://doi.org/10.1007/978-1-4939-8879-2_26 PMID: 30378064

73. Ashby MC, Camello-Almaraz C, Gerasimenko OV, Petersen OH, Tepikin AV. Long distance communication between muscarinic receptors and Ca2+ release channels revealed by carbachol uncaging in cell-attached patch pipette. J Biol Chem. 2003; 278: 20860–20864. https://doi.org/10.1074/jbc.M302599200 PMID: 12657637

74. Perc M, Rupnik M, Gosak M, Marhl M. Prevalence of stochasticity in experimentally observed responses of pancreatic acinar cells to acetylcholine. Chaos Woodbury N. 2009; 19: 037113. https://doi.org/10.1063/1.3160017 PMID: 19792038

75. Skelin M, Rupnik M. cAMP increases the sensitivity of exocytosis to Ca^2+ primarily through protein kinase A in mouse pancreatic beta cells. Cell Calcium. 2011; 49: 89–99. https://doi.org/10.1016/j.ceca.2010.12.005 PMID: 21242000

76. Poole CA, Brookes NH, Clover GM. Keratocyte networks visualised in the living cornea using vital dyes. J Cell Sci. 1993; 106 (Pt 2): 685–691. https://doi.org/10.1242/jcs.106.2.685 PMID: 8282773

77. Lock JT, Parker I, Smith IF. A comparison of fluorescent Ca^{2+} indicators for imaging local Ca^{2+} signals in cultured cells. Cell Calcium. 2015; 58: 638–648. https://doi.org/10.1016/j.ceca.2015.10.003 PMID: 26572560

78. Tada M, Takeuchi A, Hashizume M, Kitamura K, Kano M. A highly sensitive fluorescent indicator dye for calcium imaging of neural activity in vitro and in vivo. Eur J Neurosci. 2014; 39: 1720–1728. https://doi.org/10.1111/ejn.12476 PMID: 24405482

79. Dodt H-U, Becker K, Zieglgänsberger W. Infrared video microscopy for visualizing neurons and neuronal excitation in brain slices. Cold Spring Harb Protoc. 2013; 2013: 1149–1152. https://doi.org/10.1101/pdb.prot079434 PMID: 24298032

80. Chacron MJ, Longtin A, Maler L. Negative interspike interval correlations increase the neuronal capacity for encoding time-dependent stimuli. J Neurosci Off J Soc Neurosci. 2001; 21: 5328–5343. https://doi.org/10.1523/JNEUROSCI.21-14-05328.2001 PMID: 11438609

81. Hodson DJ, Schaeffer M, Romanò N, Fontanaud P, Lafont C, Birkenstock J, et al. Existence of long-lasting experience-dependent plasticity in endocrine cell networks. Nat Commun. 2012; 3: 605. https://doi.org/10.1038/ncomms1612 PMID: 22215080

82. Gosak M, Markovič R, Dolenšek J, Slak Rupnik M, Marhl M, Stožer A, et al. Network science of biological systems at different scales: A review. Phys Life Rev. 2018; 24: 118–135. https://doi.org/10.1016/j.plrev.2017.11.003 PMID: 29150402

83. Cleveland M, Sawyer JM, Afelik S, Jensen J, Leach SD. Exocrine ontogenies: On the development of pancreatic acinar, ductal and centroacinar cells. Semin Cell Dev Biol. 2012; 23: 711–719. https://doi.org/10.1016/j.semcdb.2012.06.008 PMID: 22743232

84. Kattner N, Dyson N, Bury Y, Tiniakos D, White K, Davey T, et al. Development and validation of a quantitative electron microscopy score to assess acute cellular stress in the human exocrine pancreas. J Pathol Clin Res. n/a. https://doi.org/10.1002/cjp2.185 PMID: 33225596

85. Beheiry RR, Salem HF, Karkit MW. Ultrastructural studies on the pancreatic acini in duck (Anas boscas) and pigeon (Columba livia). Anat Histol Embryol. 2020; 49: 345–350. https://doi.org/10.1111/ahe.12533 PMID: 32017197

86. Inagaki T, Tajiri T, Tate G, Kunimura T, Morohoshi T. Dynamic morphologic change and differentiation from fetal to mature pancreatic acinar cells in rats. J Nippon Med Sch Nippon Ika Daigaku Zasshi. 2012; 79: 335–342. https://doi.org/10.1272/jnms.79.335 PMID: 23123389

87. Beheiry RR, Abdel-Raheem WA-A, Balah AM, Salem HF, Karkit MW. Morphological, histological and ultrastructural studies on the exocrine pancreas of goose. Beni-Suef Univ J Basic Appl Sci. 2018; 7: 353–358. https://doi.org/10.1016/j.bjbas.2018.03.009

88. Tarnowski BI, Spinale FG, Nicholson JH. DAPI as a useful stain for nuclear quantitation. Biotech Histochem Off Publ Biol Stain Comm. 1991; 66: 297–302. PMID: 1725854

89. Williams JA. Amylase. Pancreapedia Exocrine Pancreas Knowl Base. 2019. https://doi.org/10.3998/panc.2019.02 Available from: https://www.pancreapedia.org/molecules/amylase-2

90. Yule DI, Gallacher DV. Oscillations of cytosolic calcium in single pancreatic acinar cells stimulated by acetylcholine. FEBS Lett. 1988; 239: 358–362. https://doi.org/10.1016/0014-5793(88)80951-7 PMID: 3141216

91. Yule DI, Lawrie AM, Gallacher DV. Acetylcholine and cholecystokinin induce different patterns of oscillating calcium signals in pancreatic acinar cells. Cell Calcium. 1991; 12: 145–151. https://doi.org/10.1016/0143-4160(91)90016-8 PMID: 2059990

92. Stožer A, Skelin Klemen M, Gosak M, Križančić Bombek L, Pohorec V, Slak Rupnik M, et al. Glucose-dependent activation, activity, and deactivation of beta cell networks in acute mouse pancreas tissue slices. Am J Physiol Endocrinol Metab. 2021; 321: E305–E323. https://doi.org/10.1152/ajpendo.00043.2021 PMID: 34280052

93. Tsunoda Y, Stuenkel EL, Williams JA. Oscillatory mode of calcium signaling in rat pancreatic acinar cells. Am J Physiol. 1990; 258: C147–155. https://doi.org/10.1152/ajpcell.1990.258.1.C147 PMID: 2301562

94. LeBeau AP, Yule DI, Groblewski GE, Sneyd J. Agonist-dependent phosphorylation of the inositol 1,4,5-trisphosphate receptor: A possible mechanism for agonist-specific calcium oscillations in pancreatic acinar cells. J Gen Physiol. 1999; 113: 851–872. https://doi.org/10.1085/jgp.113.6.851 PMID: 10352035

95. Dolai S, Takahashi T, Qin T, Liang T, Xie L, Kang F, et al. Pancreas-specific SNAP23 depletion prevents pancreatitis by attenuating pathological basolateral exocytosis and formation of trypsin-activating autolysosomes. Autophagy. 2020; 1–14. https://doi.org/10.1080/15548627.2020.1852725

96. Grubelnik V, Markovič R, Lipovšek S, Leitinger G, Gosak M, Dolenšek J, et al. Modelling of dysregulated glucagon secretion in type 2 diabetes by considering mitochondrial alterations in pancreatic α-cells. R Soc Open Sci. 2020; 7: 191171. https://doi.org/10.1098/rsos.191171 PMID: 32218947

97. Qadir MMF, Álvarez-Cubela S, Weitz J, Panzer JK, Klein D, Moreno-Hernández Y, et al. Long-term culture of human pancreatic slices as a model to study real-time islet regeneration. Nat Commun. 2020; 11: 3265. https://doi.org/10.1038/s41467-020-17040-8 PMID: 32601271

98. Toescu EC, Gardner JM, Petersen OH. Mitochondrial Ca2+ uptake at submicromolar [Ca2+]i in permeabilised pancreatic acinar cells. Biochem Biophys Res Commun. 1993; 192: 854–859. https://doi.org/10.1006/bbrc.1993.1493 PMID: 8484790

99. Elliott AC, Bruce JI. Analysis of calcium oscillations in pancreatic acinar cells. Digestion. 1997; 58 Suppl 2: 69–74. https://doi.org/10.1159/000201547 PMID: 9302494

100. Sluga N, Postić S, Sarikas S, Huang Y-C, Stožer A, Slak Rupnik M. Dual Mode of Action of Acetylcholine on Cytosolic Calcium Oscillations in Pancreatic Beta and Acinar Cells In Situ. Cells. 2021; 10: 1580. https://doi.org/10.3390/cells10071580 PMID: 34201461

101. Stuenkel EL, Tsunoda Y, Williams JA. Secretagogue induced calcium mobilization in single pancreatic acinar cells. Biochem Biophys Res Commun. 1989; 158: 863–869. https://doi.org/10.1016/0006-291x(89)92802-7 PMID: 2920043

102. Petersen OH, Tepikin AV, Gerasimenko JV, Gerasimenko OV, Sutton R, Criddle DN. Fatty acids, alcohol and fatty acid ethyl esters: toxic Ca2+ signal generation and pancreatitis. Cell Calcium. 2009; 45: 634–642. https://doi.org/10.1016/j.ceca.2009.02.005 PMID: 19327825

103. Habara Y, Kanno T. Stimulus-secretion coupling and Ca2+ dynamics in pancreatic acinar cells. Gen Pharmacol. 1994; 25: 843–850. https://doi.org/10.1016/0306-3623(94)90085-x PMID: 7835627

104. Pralong WF, Wollheim CB, Bruzzone R. Measurement of cytosolic free Ca2+ in individual pancreatic acini. FEBS Lett. 1988; 242: 79–84. https://doi.org/10.1016/0014-5793(88)80989-x PMID: 2462514

105. Campos-Toimil M, Edwardson JM, Thomas P. Real-time studies of zymogen granule exocytosis in intact rat pancreatic acinar cells. J Physiol. 2000; 528 Pt 2: 317–326. https://doi.org/10.1111/j.1469-7793.2000.00317.x PMID: 11034621

106. Wäsle B, Edwardson JM. The regulation of exocytosis in the pancreatic acinar cell. Cell Signal. 2002; 14: 191–197. https://doi.org/10.1016/s0898-6568(01)00257-1 PMID: 11812646

107. Messenger SW, Falkowski MA, Groblewski GE. Ca^{2+}-regulated secretory granule exocytosis in pancreatic and parotid acinar cells. Cell Calcium. 2014; 55: 369–375. https://doi.org/10.1016/j.ceca.2014.03.003 PMID: 24742357

108. Campos-Toimil M, Bagrij T, Edwardson JM, Thomas P. Two modes of secretion in pancreatic acinar cells: involvement of phosphatidylinositol 3-kinase and regulation by capacitative Ca(2+) entry. Curr Biol CB. 2002; 12: 211–215. https://doi.org/10.1016/s0960-9822(01)00661-3 PMID: 11839273

109. Osipchuk YV, Wakui M, Yule DI, Gallacher DV, Petersen OH. Cytoplasmic Ca2+ oscillations evoked by receptor stimulation, G-protein activation, internal application of inositol trisphosphate or Ca2+: simultaneous microfluorimetry and Ca2+ dependent Cl- current recording in single pancreatic acinar cells. EMBO J. 1990; 9: 697–704. https://doi.org/10.1002/j.1460-2075.1990.tb08162.x PMID: 1690123

110. Dai JM, Kuo K-H, Leo JM, Paré PD, van Breemen C, Lee C-H. Acetylcholine-induced asynchronous calcium waves in intact human bronchial muscle bundle. Am J Respir Cell Mol Biol. 2007; 36: 600–608. https://doi.org/10.1165/rcmb.2006-0096OC PMID: 17170384

111. Roux E, Guibert C, Savineau JP, Marthan R. [Ca2+]i oscillations induced by muscarinic stimulation in airway smooth muscle cells: receptor subtypes and correlation with the mechanical activity. Br J Pharmacol. 1997; 120: 1294–1301. https://doi.org/10.1038/sj.bjp.0701061 PMID: 9105705

112. Wang J, Verchere CB, McIntosh CH, Brown JC. Characterization of acetylcholine-induced increases in cytosolic free calcium concentration in individual rat pancreatic beta-cells. Cell Adhes Commun. 1994; 1: 343–353. https://doi.org/10.3109/15419069409097265 PMID: 8081885

113. Willems PH, Van Emst-De Vries SE, Van Os CH, De Pont JJ. Dose-dependent recruitment of pancreatic acinar cells during receptor-mediated calcium mobilization. Cell Calcium. 1993; 14: 145–159. https://doi.org/10.1016/0143-4160(93)90084-j PMID: 7681361

114. Wang J, Wang Y, Guo F, Feng Z, Wang X, Lu C. Nicotinic modulation of Ca2+ oscillations in rat cortical neurons in vitro. Am J Physiol Cell Physiol. 2016; 310: C748–754. https://doi.org/10.1152/ajpcell.00197.2015 PMID: 26843531

115. Jacob R, Merritt JE, Hallam TJ, Rink TJ. Repetitive spikes in cytoplasmic calcium evoked by histamine in human endothelial cells. Nature. 1988; 335: 40–45. https://doi.org/10.1038/335040a0 PMID: 3412458

116. Rooney TA, Sass EJ, Thomas AP. Characterization of cytosolic calcium oscillations induced by phenylephrine and vasopressin in single fura-2-loaded hepatocytes. J Biol Chem. 1989; 264: 17131–17141. PMID: 2793847

117. Verma A, Antony AN, Ogunnaike BA, Hoek JB, Vadigepalli R. Causality Analysis and Cell Network Modeling of Spatial Calcium Signaling Patterns in Liver Lobules. Front Physiol. 2018; 9: 1377. https://doi.org/10.3389/fphys.2018.01377 PMID: 30337879

118. Resende RR, Adhikari A, da Costa JL, Lorençon E, Ladeira MS, Guatimosim S, et al. Influence of spontaneous calcium events on cell-cycle progression in embryonal carcinoma and adult stem cells. Biochim Biophys Acta. 2010; 1803: 246–260. https://doi.org/10.1016/j.bbamcr.2009.11.008 PMID: 19958796

119. Sauer H, Hofmann C, Wartenberg M, Wobus AM, Hescheler J. Spontaneous calcium oscillations in embryonic stem cell-derived primitive endodermal cells. Exp Cell Res. 1998; 238: 13–22. https://doi.org/10.1006/excr.1997.3809 PMID: 9457052

120. Shitara A, Tanimura A, Sato A, Tojyo Y. Spontaneous oscillations in intracellular Ca(2+) concentration via purinergic receptors elicit transient cell swelling in rat parotid ducts. Am J Physiol Gastrointest Liver Physiol. 2009; 297: G1198–1205. https://doi.org/10.1152/ajpgi.00168.2009 PMID: 19779019

121. Vukcevic M, Zorzato F, Spagnoli G, Treves S. Frequent calcium oscillations lead to NFAT activation in human immature dendritic cells. J Biol Chem. 2010; 285: 16003–16011. https://doi.org/10.1074/jbc.M109.066704 PMID: 20348098

122. Balaji R, Bielmeier C, Harz H, Bates J, Stadler C, Hildebrand A, et al. Calcium spikes, waves and oscillations in a large, patterned epithelial tissue. Sci Rep. 2017; 7: 42786. https://doi.org/10.1038/srep42786 PMID: 28218282

123. Zhou Y, Lv M, Li T, Zhang T, Duncan R, Wang L, et al. Spontaneous calcium signaling of cartilage cells: from spatiotemporal features to biophysical modeling. FASEB J Off Publ Fed Am Soc Exp Biol. 2019; 33: 4675–4687. https://doi.org/10.1096/fj.201801460R PMID: 30601690

124. Kawano S, Otsu K, Kuruma A, Shoji S, Yanagida E, Muto Y, et al. ATP autocrine/paracrine signaling induces calcium oscillations and NFAT activation in human mesenchymal stem cells. Cell Calcium. 2006; 39: 313–324. https://doi.org/10.1016/j.ceca.2005.11.008 PMID: 16445977

125. Vincze J, Geyer N, Diszházi G, Csernoch L, Bíró T, Jóna I, et al. Laser induced calcium oscillations in fluorescent calcium imaging. Gen Physiol Biophys. 2018; 37: 253–261. https://doi.org/10.4149/gpb_2017054 PMID: 29589836

126. Jaffe LF. Stretch-activated calcium channels relay fast calcium waves propagated by calcium-induced calcium influx. Biol Cell. 2007; 99: 175–184. https://doi.org/10.1042/BC20060031 PMID: 17302561

127. Michon L, Nlend Nlend R, Bavamian S, Bischoff L, Boucard N, Caille D, et al. Involvement of gap junctional communication in secretion. Biochim Biophys Acta. 2005; 1719: 82–101. https://doi.org/10.1016/j.bbamem.2005.11.003 PMID: 16359942

128. Dupont G, Combettes L. What can we learn from the irregularity of Ca2+ oscillations? Chaos Woodbury N. 2009; 19: 037112. https://doi.org/10.1063/1.3160569 PMID: 19792037

129. Dupont G, Abou-Lovergne A, Combettes L. Stochastic aspects of oscillatory Ca2+ dynamics in hepatocytes. Biophys J. 2008; 95: 2193–2202. https://doi.org/10.1529/biophysj.108.133777 PMID: 18515398

130. Romano SA, Pérez-Schuster V, Jouary A, Boulanger-Weill J, Candeo A, Pietri T, et al. An integrated calcium imaging processing toolbox for the analysis of neuronal population dynamics. PLoS Comput Biol. 2017; 13: e1005526. https://doi.org/10.1371/journal.pcbi.1005526 PMID: 28591182

131. Rueckl M, Lenzi SC, Moreno-Velasquez L, Parthier D, Schmitz D, Ruediger S, et al. SamuROI, a Python-Based Software Tool for Visualization and Analysis of Dynamic Time Series Imaging at Multiple Spatial Scales. Front Neuroinformatics. 2017; 11: 44. https://doi.org/10.3389/fninf.2017.00044 PMID: 28706482

132. Sneyd J, Tsaneva-Atanasova K, Bruce JIE, Straub SV, Giovannucci DR, Yule DI. A model of calcium waves in pancreatic and parotid acinar cells. Biophys J. 2003; 85: 1392–1405. https://doi.org/10.1016/S0006-3495(03)74572-X PMID: 12944257

133. Manhas N, Sneyd J, Pardasani KR. Modelling the transition from simple to complex Ca^{2+} oscillations in pancreatic acinar cells. J Biosci. 2014; 39: 463–484. https://doi.org/10.1007/s12038-014-9430-3 PMID: 24845510

134. Tsaneva-Atanasova K, Yule DI, Sneyd J. Calcium Oscillations in a Triplet of Pancreatic Acinar Cells. Biophys J. 2005; 88: 1535–1551. https://doi.org/10.1529/biophysj.104.047357 PMID: 15596494

135. Rose T, Efendic S, Rupnik M. Ca2+-secretion coupling is impaired in diabetic Goto Kakizaki rats. J Gen Physiol. 2007; 129: 493–508. https://doi.org/10.1085/jgp.200609604 PMID: 17535961

136. Paschen M, Moede T, Valladolid-Acebes I, Leibiger B, Moruzzi N, Jacob S, et al. Diet-induced β-cell insulin resistance results in reversible loss of functional β-cell mass. FASEB J Off Publ Fed Am Soc Exp Biol. 2019; 33: 204–218. https://doi.org/10.1096/fj.201800826R PMID: 29957055

137. Yang X, Yao L, Fu X, Mukherjee R, Xia Q, Jakubowska MA, et al. Experimental Acute Pancreatitis Models: History, Current Status, and Role in Translational Research. Front Physiol. 2020; 11: 614591. https://doi.org/10.3389/fphys.2020.614591 PMID: 33424638

138. Cohrs CM, Panzer JK, Drotar DM, Enos SJ, Kipke N, Chen C, et al. Dysfunction of Persisting β Cells Is a Key Feature of Early Type 2 Diabetes Pathogenesis. Cell Rep. 2020; 31: 107469. https://doi.org/10.1016/j.celrep.2020.03.033 PMID: 32268101

139. Cohrs CM, Chen C, Jahn SR, Stertmann J, Chmelova H, Weitz J, et al. Vessel Network Architecture of Adult Human Islets Promotes Distinct Cell-Cell Interactions In Situ and Is Altered After Transplantation. Endocrinology. 2017; 158: 1373–1385. https://doi.org/10.1210/en.2016-1184 PMID: 28324008

140. Fernandez NA, Liang T, Gaisano HY. Live pancreatic acinar imaging of exocytosis using syncollin-pHluorin. Am J Physiol Cell Physiol. 2011; 300: C1513–1523. https://doi.org/10.1152/ajpcell.00433.2010 PMID: 21307342

141. Nemoto T, Kimura R, Ito K, Tachikawa A, Miyashita Y, Iino M, et al. Sequential-replenishment mechanism of exocytosis in pancreatic acini. Nat Cell Biol. 2001; 3: 253–258. https://doi.org/10.1038/35060042 PMID: 11231574

142. Thorn P, Parker I. Two phases of zymogen granule lifetime in mouse pancreas: ghost granules linger after exocytosis of contents. J Physiol. 2005; 563: 433–442. https://doi.org/10.1113/jphysiol.2004.077230 PMID: 15637100

143. Thorn P, Fogarty KE, Parker I. Zymogen granule exocytosis is characterized by long fusion pore openings and preservation of vesicle lipid identity. Proc Natl Acad Sci U S A. 2004; 101: 6774–6779. https://doi.org/10.1073/pnas.0400336101 PMID: 15090649

144. Skelin Klemen M, Dolenšek J, Stožer A, Slak Rupnik M. Measuring Exocytosis in Endocrine Tissue Slices. In: Thorn P, editor. Exocytosis Methods. Totowa, NJ: Humana Press; 2014. pp. 127–146. https://doi.org/10.1007/978-1-62703-676-4_7

145. Hegyi P, Petersen OH. The exocrine pancreas: the acinar-ductal tango in physiology and pathophysiology. Rev Physiol Biochem Pharmacol. 2013; 165: 1–30. https://doi.org/10.1007/112_2013_14 PMID: 23881310